Ternary Organic Solar Cells with Minimum Voltage Losses

Chuanfei Wang, Wei Zhang, Xiangyi Meng, Jonas Bergqvist, Xianjie Liu, Zewdneh Genene, Xiaofeng Xu, Arkady Yartsev, Olle Inganäs, Wei Ma, Ergang Wang and Mats Fahlman

Wang, C., Zhang, W., Meng, X., Bergqvist, J., Liu, X., Genene, Z., Xu, X., Yartsev, A., Inganäs, O., Ma, W., Wang, E., Fahlman, M., (2017), Ternary Organic Solar Cells with Minimum Voltage Losses, *Advanced Energy Materials*, 7(21), . https://doi.org/10.1002/aenm.201700390

Original publication available at:
https://doi.org/10.1002/aenm.201700390

DOI: 10.1002/ ((please add manuscript number))
Article type: Full Paper

Ternary Organic Solar Cells with Minimum Voltage Losses

Chuanfei Wang, Wei Zhang, Xiangyi Meng, Jonas Bergqvist, Xianjie Liu, Zewdneh Genene, Xiaofeng Xu, *Arkady Yartsev, Olle Inganäs, Wei Ma, Ergang Wang, Mats Fahlman**

C. Wang, Author 1, Dr. X. Liu, Author5, Prof. M. Fahlman, Author 12.
Division of Surface Physics and Chemistry, IFM, Linköping University, SE-581 83 Linköping, Sweden
E-mail: mats.fahlman@liu.se

Dr. W. Zhang, Author 2, Prof. A. Yartsev, Author 8
Division of Chemical Physics, Lund University, Box 124, 221 00 Lund, Sweden

X. Meng, Author 3, Prof. W. Ma, Author 10.
State Key Laboratory for Mechanical Behavior of Materials, Xi'an Jiaotong University, Xi'an 710049, China

Dr. J. Bergqvist, Author 4, Prof. Olle Inganäs, Author 9
Biomolecular and Organic Electronics, IFM, Linköping University, SE-581 83 Linköping, Sweden

Z. Genene, Author6.
Department of Chemistry, Addis Ababa University, P.O. Box 33658, Addis Ababa, Ethiopia

Z. Genene, Author6, Dr. Xiaofeng Xu, Author7, Dr. Ergang Wang, Author 11
Department of Chemistry and Chemical Engineering, Chalmers University of Technology, SE-412 96 Göteborg, Sweden

Keywords: Ternary Solar Cell, Same Bulk and Interface Energy, Binary Equivalent, Minimum Voltage losses

Abstract: A new strategy for designing ternary solar cells is disclosed in this contribution. We select a low bandgap polymer named PTB7-Th and a high band gap polymer named PBDTTS-FTAZ sharing the same bulk ionization potential and interface positive integer charge transfer energy while featuring complementary absorption spectra. They are used to fabricate efficient ternary solar cells, where the hole can be transported freely between the two donor polymers and collected by the electrode as in one broadband low bandgap polymer. Furthermore, the fullerene acceptor is chosen so that the energy of the positive integer charge transfer state of the two donor polymers is equal to the energy of negative integer charge transfer state of the fullerene, enabling enhanced dissociation of all polymer donor and fullerene acceptor excitons and suppressed bimolecular and trap assistant recombination. The

two donor polymers feature good miscibility and energy transfer from high bandgap polymer of PBDTTS-FTAZ to low bandgap polymer of PTB7-Th, which contribute to enhanced performance of the ternary solar cell.

1. Introduction

The overall power conversion efficiency (PCE) of organic bulk heterojunction (BHJ) solar cells depends on the open circuit voltage (V_{oc}), short circuit current density (J_{sc}), fill factor (FF) and power of the incident irradiation (P_{in}) and can be formulated as PCE = $J_{sc}V_{oc}FF/P_{in}$. According to this formula, it is clear that voltage losses ($V_{oc\ loss}$) should be minimized and J_{sc} should be maximized. $V_{oc\ loss}$ can be reduced by optimization of energetics at all interfaces[1, 2] and the energy level alignment at the various interfaces in BHJ devices can be predicted using the Integer Charge Transfer (ICT) model.[3] The ICT model states that spontaneous charge transfer across an interface will occur when the substrate work function is larger (smaller) than the energy required to oxide (gained form reducing) a molecule/polymer at the interface forming Integer Charge Transfer states. Note that these Interface Charge Transfer states typically do not have the same energy as bulk polarons, mainly due to Coulombic interaction with the opposite charge across the interface (see **Figure S1**). The most easily oxidized/reduced molecules adjacent to the interface are used up in the process until enough charge has been transferred across the interface to create a potential step that equilibrates the Fermi level. The resulting pinning energies are referred as the $E_{ICT+,-}$ depending on if it is positive or negative polarons created in the organic semiconductor material (see supporting information for more details). The so-called pinning energies, $E_{ICT+,-}$, thus can be used to predict ground state charge transfer and potential energy gradients at interfaces (or absence thereof),[4] and can be obtained experimentally using *e.g.* photoelectron spectroscopy[5] or Kelvin probe measurements,[6] as well as theoretically using a wide variety of computational techniques.[7, 8, 9, 10, 11] The work function of the typically used anode (PEDOT: PSS) and cathode (LiF/Al) is sufficiently large[12] (small)[13] to form pinned contacts with the donor

(acceptor) materials in BHJ devices. Charge transfer exciton dissociation and charge recombination mainly takes place at the BHJ interface, however, and both processes affect $V_{oc\ loss}$.[1, 14] Occupied Integer Charge Transfer states at the donor/acceptor (D/A) interface, occurring when $E_{ICT+,\ D} \leq E_{ICT-,\ A}$ (**Figure 1**), can act as trap sites for recombination that reduce the V_{oc}, while the generation of free charges at the D/A interface is enhanced by the interface potential energy gradient generated by occupied Integer Charge Transfer states.[1, 15, 16] Hence, there is a trade-off in terms of occupied Integer Charge Transfer state density and the sweet spot occurs at $E_{ICT-,\ A} \approx E_{ICT+,D}$,[1] see also supporting information. J_{sc} can be increased through enhancements in photon absorption, charge transfer exciton dissociation and/or reduction of free charge recombination.[14] Ternary organic solar cells can tune the light absorption intensity in different wavelength regions[17, 18, 19, 20] and hence potentially increase photon absorption in the device, but recent modeling of two donor ternary devices suggest that for state of the art absorbers featuring broad and strong absorption spectra, the ternary approach offers no improvement unless the ternary blend enhances transport and/or recombination kinetics.[21] Nevertheless, the ternary solar cell approach has been approved an efficient method to improve the performance of organic solar cell[22, 23, 24, 25, 26, 27] and has yielded > 10% PCE.[28, 29, 30, 31, 32, 33, 34] The path forward towards increased PCE should involve maintaining the exciton generation efficiency of the binary blends while using the ternary system to improve exciton dissociation and transport. The introduction of the third light-absorbing component (donor or acceptor) introduces additional kinds of interfaces that may act as trap sites,[17, 35] limiting charge transport in the device. If however the two donor polymers have same bulk ionization potential (*IP*)[18] and positive pinning energy (E_{ICT+}), hole-transport can occur freely between and through the domains formed by the different donors, essentially making the ternary solar cells work as a binary one. (For a two acceptor - one donor ternary device the acceptor electron affinities and negative pinning energy (E_{ICT-}) should be matched to achieve the same effect). We follow this approach and combine two

efficient donor polymers with same *IP* and E_{ICT+} in a ternary device with $PC_{71}BM$. We show that the current density is increased due to enhanced exciton dissociation efficiency and lower (bimolecular) recombination during transport, due to the chosen donor/acceptor interface energetics as well as the formation of multi-scale phase separation [36] in the ternary blends. The complimentary absorption from the secondary donor is shown to compensate for the loss in absorption from the primary donor, but does not in itself enhance overall photocurrent, in line with the result from modeling.[21] We further demonstrate that the $V_{oc\ loss}$ is minimized when using two donor polymers with the same positive pinning energy that is equal to negative pinning energy of the fullerene acceptor. The fill factor is maintained at a high level in spite of intermixing of the donors as also the ionization potential of two donor polymers are equal. We finally show that efficient energy transfer and charge transfer coexist between the two donor polymers with same ionization potential and positive pinning energy.

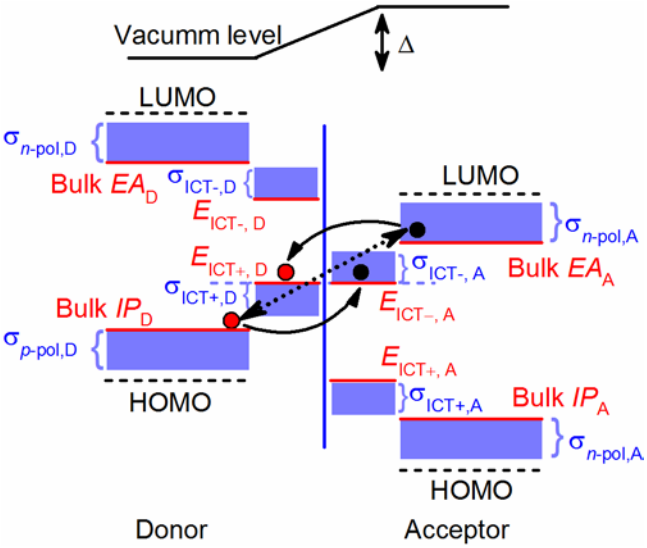

Figure 1: Energy level alignement between adjacent donor and acceptor when $E_{ICT+,D} \leq E_{ICT-,A}$. σ represents the distribution of ICT, *IP* and *EA*. $\Delta = E_{ICT-,\,A} - E_{ICT+,D}$ represent interface potential step caused by Femi level equilibrium. Solid arrow represent direct bimolecular recombination and dashed arrow represent trap assistant recombination via ICT state.

2. Results and Discussions

PTB7-Th is a well-known donor polymer that combined with fullerenes in BHJ solar cells gives PCE of around 7.5% in conventional devices[37, 38] and around 10% in inverted devices.[39] Because of the excellent photovoltaic properties of PTB7-Th, it is also used as donor polymer in non-fullerene binary solar cells [40] and as the host donor polymer in ternary solar cells.[2, 28, 37, 41] A high bandgap polymer named PBDTTS-FTAZ (**Scheme 1**) designed for tandem solar cells[42, 43, 44] has a complementary absorption to PTB7-Th, see **Figure 2a**, and can thus be used as a second donor component in ternary solar cells. The high bandgap polymer PBDTTS-FTAZ exhibits narrow and strong absorption in the wavelength region from 450 to 650 nm, while the low bandgap polymer PTB7-Th exhibit absorption in the wavelength region from 500 to 780 nm. When these two donor polymers are blended together, a series of new complementary absorption spectrum can be obtained and the absorption intensity can be tuned through different ratios of two donors as shown in the absorption spectrum of two donor polymers with different weight ratio (**Figure S2c**) and in the absorption spectrum of the ternary blends (**Figure2b**). With increasing content of PBDTTS-FTAZ, the absorption between 600nm to 780nm in the ternary blends was decreased gradually, while the absorption between 450nm to 600 nm was increased gradually, which is consistent with the individual complementary absorption of the two donor polymers.

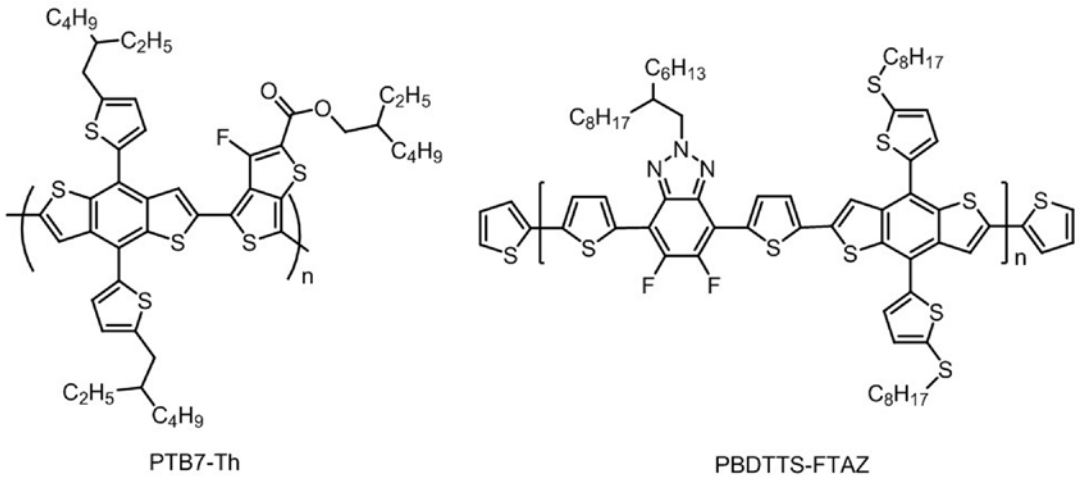

Scheme 1. Chemical structure of PTB7-Th and PBDTTS-FTAZ

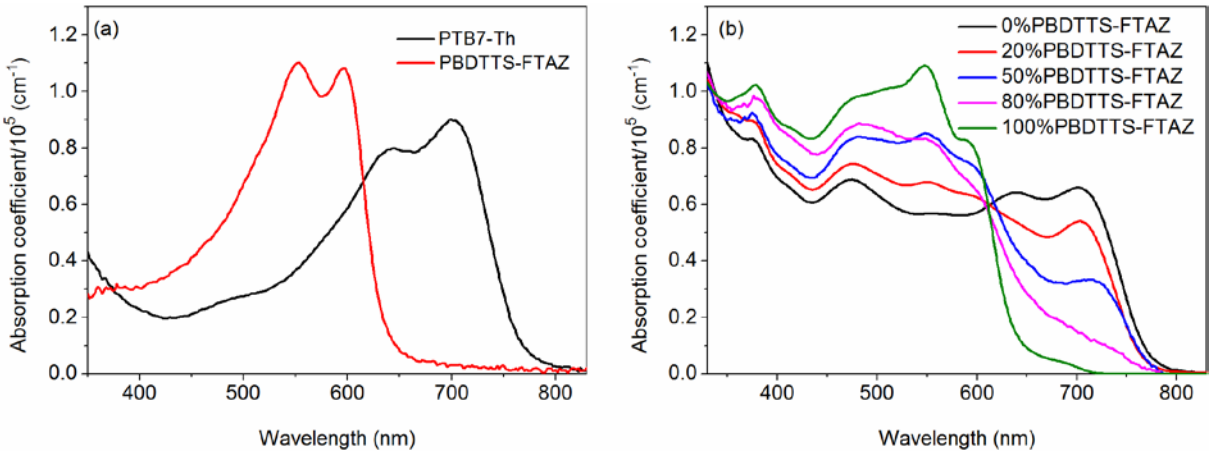

Figure 2. a) UV-vis absorption spectrum of PTB7-Th, PBDTTS-FTAZ neat films. b) UV-vis absorption spectrum of ternary blends with different PBDTTS-FTAZ contents. The D-A ratio is 1:1.5 for all ternary blends and the percentages given refer to the relative concentration of PBDTTS-FTAZ *vs.* PTB7-Th.

The energy levels related to hole and electron transport can be measured by either ultra violet photoelectron spectroscopy (UPS) or cyclic voltammetry (CV) method. In our study, UPS is used to measure ionization potential and pinning energy of the donor and acceptor materials and the values are listed in **Table S1**. The *IP* of two donor polymers are the same, 4.85 eV, and they also have same positive pinning energy, 4.35 eV, as shown in **Figure 3a** and **Table S1**. Note that positive pinning energy of the two donor polymers ($E_{ICT+,\ D}$) is also equal to negative pinning energy of the $PC_{71}BM$ acceptor ($E_{ICT-,\ A}$ = 4.35 eV) as shown in **Figure S3c** and **Table S1,** *i.e.* $E_{\ ICT+,\ D} \approx E_{ICT-,\ A}$ = 4.35 eV, which then should yield the optimized D/A energetics for both donors in terms of minimizing $V_{oc\ loss}$. $V_{oc\ loss}$ is here defined as the deviation from the ideal V_{oc} ($\Delta E_{g,\ eff}^{DA}$) in the measured V_{oc}, which can be formulated as $eV_{oc,\ loss} = \Delta E_{g,\ eff}^{DA} - eV_{oc}$. $\Delta E_{g,\ eff}^{DA}$ is the effective difference between the ionization potential (IP_D) of the donor and the electron affinity (EA_A) of the acceptor ($IP_D - EA_A$) formulated as $\Delta E_{g,\ eff}^{DA} = IP_D - EA_A + \Delta$, where Δ is the potential energy step/gradient shifting the vacuum level at the D/A interface, see **Figure 1**.[1, 3, 7] The electron affinity value of $PC_{71}BM$ is 3.80 eV.[45] The

interface potential energy step Δ obtained from the difference between $PC_{71}BM$ and two donor polymers is ~0 eV due to $E_{ICT+,\,D} \approx E_{ICT-,\,A}$, so the $\Delta E^{DA}_{g,\,eff} = IP_D - EA_A$ = 1.05 eV for both acceptor-donor combinations in the blend. Indeed the reported V_{oc} of binary solar cell of PTB7-Th: $PC_{71}BM$ and PBDTTS-FTAZ: $PC_{71}BM$ are all around 0.80 V[42, 46] and the $V_{oc\ loss}$ is calculated as around 0.25 eV, which is consistent with the model[1] (green region of $V_{oc\ loss}$ versus $E_{ICT+,\,D} - E_{ICT-,\,A}$ shown in **Figure 3b**). PTB7-Th and PBDTTS-FTAZ hence are excellent donor polymers from an energetics standpoint when combined with $PC_{71}BM$ and indeed yield highly efficient devices.[39, 42] We expect that when these two polymers are blended together a hole can freely move through the heterogeneous domains formed by the two donors due to the identical bulk ionization potential and interface positive pinning energy. The $V_{oc\ loss}$ is expected to locate in the minimum region of **Figure 3b** because both donors have an positive pinning energy equal to the fullerene negative pinning energy ($E_{ICT+,D} \approx E_{ICT-,A}$).

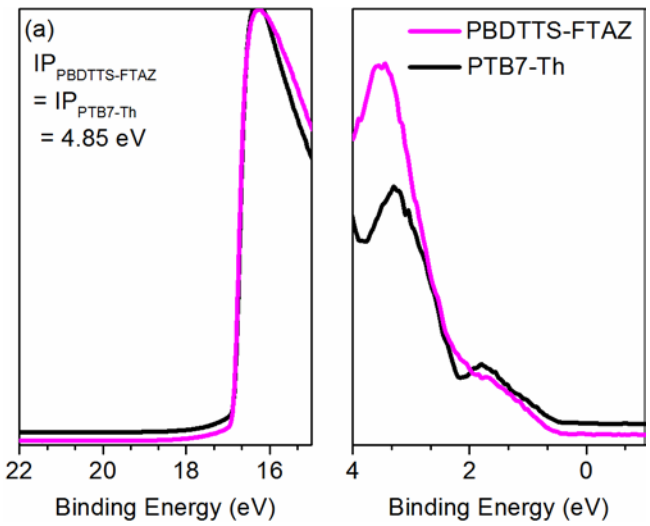

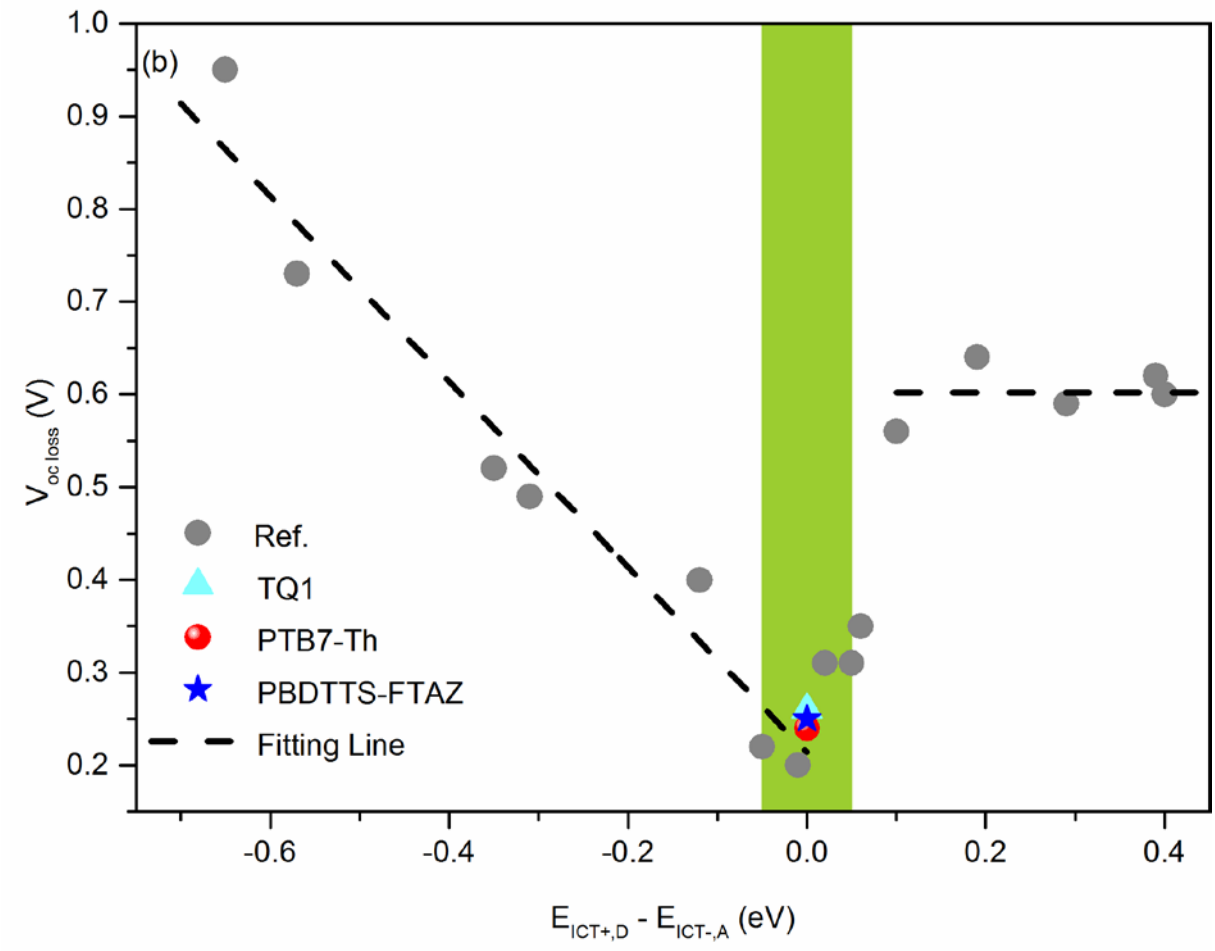

Figure 3. (a) UPS spectra of pure PTB7-Th and Pure PBDTTS-FTAZ film on the substrate of ITO/PEDOT: PSS. (b) $V_{oc\ loss}$ versus $E_{ICT+,\ D} - E_{ICT-,\ A}$ for a series of polymer: fullerene. $eV_{oc\ loss} = \Delta E_{g,\ eff}^{DA} - eV_{oc}$. The green region contains the polymer: fullerene blends where $E_{ICT+,\ D} \approx E_{ICT-,\ A}$ within the error bar of the measurement.

Our chosen ternary blend combination thus should be suitable in terms of absorption range as well as interface and bulk energetics. To test our assumptions, we fabricate ternary and binary solar cells using the conventional device structure of Glass/ITO/PEDOT: PSS/Active-layer/LiF/Al. The photovoltaic performance of the solar cells is tested in ambient atmosphere without encapsulation under simulated AM 1.5 G irradiation. The photovoltaic performance of ternary and the corresponding binary solar cells are shown in **Figure 4a** and **Table 1**. The binary solar cells of PTB7-Th: $PC_{71}BM$ show a maximum PCE of 7.7% with J_{sc} of 14.4 mA/cm^2, a V_{oc} of 0.814 V, and FF of 65.8%, which is comparable to the values reported in the

literature for the same conditions and device structure.[37, 47] Meanwhile, PBDTTS-FTAZ: $PC_{71}BM$ show a maximum PCE of 6.88% with J_{sc} of 12.05 mA/cm^2, V_{oc} of 0.799 V, and FF of 72.1%. The ionization potential and positive pinning energy of PTB7-Th and PBDTTS-FTAZ is 4.85 and 4.35eV respectively and the electron affinity and negative pinning energy of the $PC_{71}BM$ acceptor is 3.8 eV and 4.35 eV, so the $V_{oc\ loss}$ for these two binary solar cells is 0.24 eV and 0.25 eV, a minimum voltage loss due to the well matched interface energetics ($E_{ICT+,\ D} \approx E_{ICT-,\ A}$) as shown in **Figure 3b**. In the ternary solar cells, the addition of PBDTTS-FTAZ as a second donor increases the J_{sc}, FF and PCE simultaneously while maintaining the V_{oc} as high as binary solar cell as show in **Table 1**. The best photovoltaic performance is obtained when there is 20% PBDTTS-FTAZ in the blends, with a J_{sc} of 16.75 mA/cm^2, a V_{oc} of 0.813 V, FF of 67.5% and PCE of 9.2%, without use of additives or thermal annealing. The ionization potential of the two donor blend with 20% PBDTTS-FTAZ is the same as for pristine film (~4.85 eV), so the $V_{oc,\ loss}$ of optimized ternary solar cell is 0.25 eV (as we are indeed still located in the minimum voltage losses region). The V_{oc} (and $V_{oc\ loss}$) for all ternary blends stays nearly constant (**Figure S4**) as we expect from the choice of ~identical ionization potential and positive pinning energy for the two donor polymers. The FF is increased with increasing PBDTTS-FTAZ content, which we ascribe to the higher FF of PBDTTS-FTAZ: $PC_{71}BM$ binary solar cell.[42] The trend of the PCE coincides with that of the J_{sc} as shown in **Figure S4** and is enhanced for the PBDTTS-FTAZ content range of 10% to 50%.

Table 1. Device parameters of the PTB7-Th: PBDTTS-FTAZ: $PC_{71}BM$ ternary solar cells

PBDTTS-FTAZ (%)	V_{oc} (V)	J_{sc} (mA/cm^2)	FF (%)	PCE (%)	PCE (%)
0	0.814±0.003	14.4±0.3	64.0±0.9	7.5±0.15	7.7
10	0.825±0.003	15.3±0.2	66.2±1.5	8.3±0.12	8.4
20	0.816±0.006	16.4±0.1	67.3±0.9	9.0±0.12	9.2
30	0.811±0.008	15.5±0.4	68.4±1.3	8.6±0.14	8.7

50	0.817±0.004	14.6±0.2	65.1±0.8	7.8±0.13	8.0
80	0.784±0.002	12.4±0.1	69.0±0.7	6.7±0.06	6.8
100	0.792±0.007	11.7±0.4	72.3±0.5	6.7±0.12	6.9

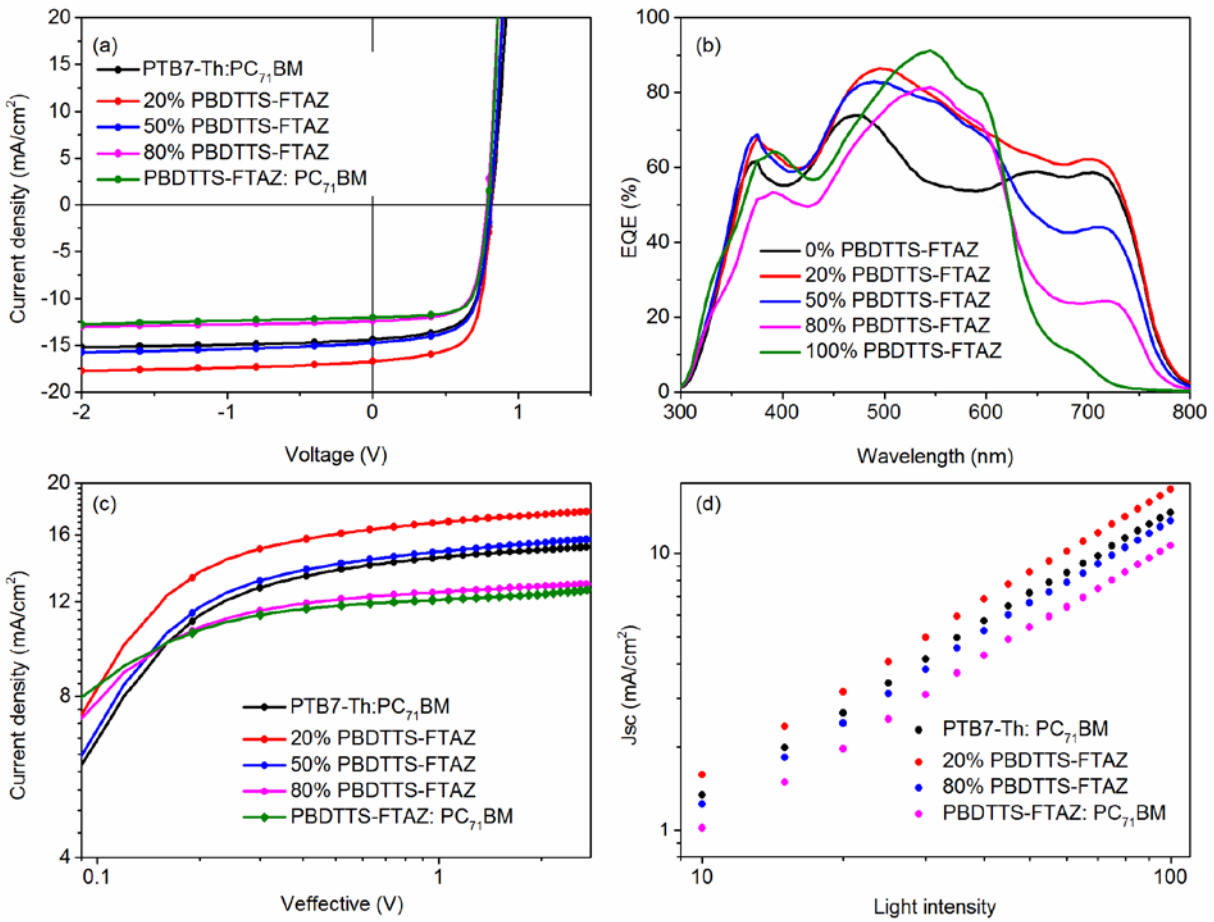

Figure 4. a) *J-V* curves of organic solar cells with different weight ratios of PBDTTS-FTAZ in the ternary blends under simulated AM 1.5 G irradiation (100 mW/cm^2) b) External quantum efficiency (EQE) curves of ternary and respective binary solar cells. c) Photocurrent density (J_{ph}) versus effective voltage (V_{eff}) characteristics. d) Dependence of J_{sc} on light intensity for ternary and related binary solar cells.

Though our ternary approach provides impressive enhancement in device efficiency, the mechanism providing the enhancement is complex. Note that in **Figure 4b**, there is an increase in the EQE for the 20% PBDTTS-FTAZ cell in the range of 600-800 nm despite that

the absorption is decreased in that region compared to the binary cells, see **Figure 2b**. The increase in J_{sc} (and PCE) must then be at least partially due to enhanced efficiency of charge generation. Indeed, more efficient charge generation is confirmed by plotting the maximum short-circuit photocurrent density ($J_{sc\text{-}max}$) as a function of the film thicknesses calculated by transfer matrix model,[48] shown in **Figure S5**. Assuming a 100% photon-to-free-charges conversion rate for all devices, the ternary with 20% PIDTTS-FTAZ and binary solar cell of PTB7-Th: $PC_{71}BM$ have near identical $J_{sc\text{-}max}$ at optimized film thickness. This suggests that the complementary absorption of the 20% PBDTTS-FTAZ merely off-sets the loss of absorption due to the reduced fraction of PTB7-Th and the enhanced J_{sc} and PCE must solely be due to more efficient charge generation and/or transport in the ternary solar cells (as expected from modeling).

For efficient ternary devices, the excitons created in the donor polymers and fullerene acceptor should be transformed into charge transfer excitons and thereafter dissociate into free charges. The potential energy step formed in dark at D/A interfaces when $E_{ICT+,A} \geq E_{ICT-,D}$ enhances the generation of free charges.[15] Furthermore, the Integer Charge Transfer states will populate the most easily oxidized polymer chains (reduced fullerene molecules) thus the most tightly bound sites where charge transfer electron-hole pairs could be created at the D/A interface are already occupied and consequently not available to participate in the exciton dissociation process following a photon absorption event, enhancing the percentage of excitons converted into free charges.[49] The exciton dissociation efficiency for both the ternary and binary blends hence are expected to be similarly high for the systems under study. We explore the exciton dissociation process of the ternary and binary solar cells by measuring photocurrent J_{ph} versus the effective V_{eff} applied voltage, which yields us the saturation circuit current ($J_{sat.}$), short circuit current (J_{sc}) and dissociation efficiency (P(E, T)) as show in **Figure 4c** and **Table S4**. The photocurrent density J_{ph} is defined as J_L-J_D, where J_L and J_D are the photocurrent densities under illumination and in the dark. The effective Voltage V_{eff} is

equal to V_0-V, where V_0 is the voltage where J_{ph} = 0 and V is the applied voltage. We assume that all the photogenerated excitons can be dissociated into free charge carriers and collected by electrodes at high bias V_{eff} (V_{eff} =2 V). The J_{sat} value of the ternary solar cells is larger than binary solar cells when the ratio of PBDTTS-FTAZ is smaller than 50%, and all the J_{sat} values are larger than the binary solar cell of PBDTTS-FTAZ: $PC_{71}BM$, which is in accordance with J_{sc} measurements. J_{ph}/J_{sat} are used to judge the charge dissociation probability (P(E,T)) and the (P(E,T)) under the J_{sc} condition are 94.6%, 94.9%, 95.4% for ternary solar cell with 20%, 50%, 80% PBDTTS-FTAZ contents, which are as high as binary solar cell of PTB7-Th: $PC_{71}BM$ (94.6%), indicating that the blending of PTB7-Th and PBDTTS-FTAZ retains an efficient exciton dissociation process as expected. High efficient dissociation also can be proved by photoluminescence (PL) quenching measurement. The PL coming from PBDTTS-FTAZ and PTB7-Th in the ternary and relative binary blend films can be quenched by $PC_{71}BM$ as shown in **Figure 5a and b**. The PL quenching efficiency is calculated according to $\Delta PL = (PL_{donor(s)}–PL_{blend})/PL_{donor(s)}$ by integrating the PL counts of each spectra in **Figure 5**. We estimate the ΔPL is around 99%, and 98% for PTB7-Th and PBDTTS-FTAZ binary solar cells. The quenching efficiency of two donors ΔPL is ~100%, ~99% and ~97% in ternary solar cells with 20%, 50% and 80% PBDTTS-FTAZ contents. Finally we probe the exciton dissociation kinetics of ternary and binary solar cells using time-resolved photoluminescence spectroscopy (TRPL). The observed PL dynamics of PBDTTS-FTAZ measured in the spectral range where only this polymer emitting is close to the instrument function in both binary and ternary blends with a weak ~10 ps component observed only in the binary blend as shown in **Figure 5c.** Thus, the PBDTTS-FTAZ exciton dissociation efficiency in the ternary blend is very high (>99%) and in the binary is slightly lower. For PTB7-Th: $PC_{71}BM$ and PBDTTS-FTAZ: $PC_{71}BM$ films, we observe a ~60 ps decay tail in the spectral range where the $PC_{71}BM$ is emissive. This PL tail is faster and its amplitude is lower in the ternary blend

(~35 ps) as shown in **Figure 5d and Table S6**. As the slower component is related to the PL decay of $PC_{71}BM$ (Supporting information and **Figure S6c**), we conclude that adding PBDTTS-FTAZ in the ternary system enhances the $PC_{71}BM$ exciton dissociation in addition to the efficient exciton dissociation in the donors. Still, as expected from the interface energetics, no dramatic enhancement is obtained and differences in exciton dissociation cannot by itself explain the improvement in ternary J_{sc} and PCE.

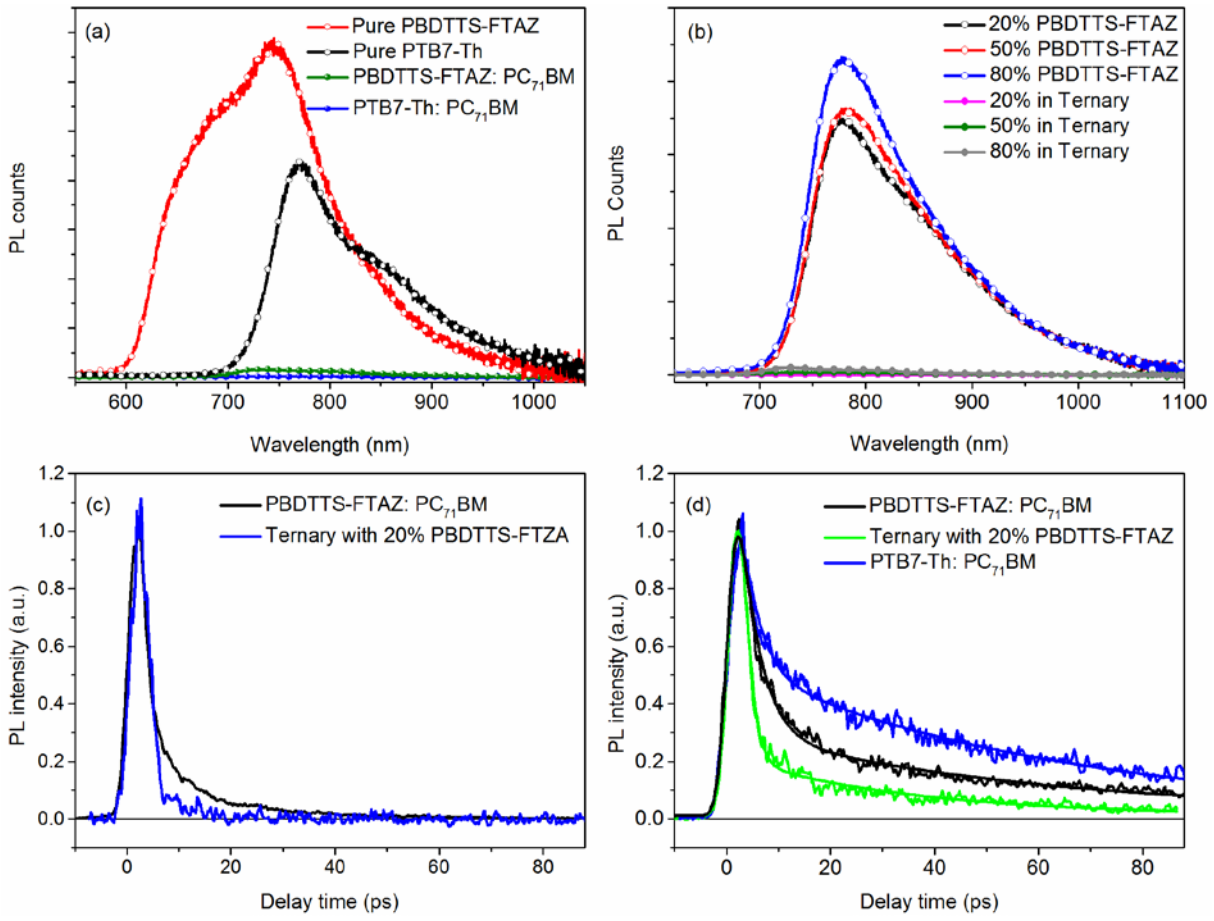

Figure 5. a) The photoluminescence spectra of neat PTB7-Th, PBDTTS-FTAZ films (open circles) and blend films with $PC_{71}BM$ (solid circles) excited at 405 nm. b) The photoluminescence spectra of PTB7-Th and PBDTTS-FTAZ films with different ratio (open circles) and blend films with $PC_{71}BM$ (solid circles) excited at 405 nm. c) TRPL kinetics of PBDTTS-FTAZ: $PC_{71}BM$ and ternary blend with 20% PBDTTS-FTAZ at 640 nm. d) TRPL kinetics of binary blend film and ternary blend with 20% PBDTTS-FTAZ at 740 nm.

Enhanced transport of the free charges to the electrodes is the other factor that can contribute to the improved J_{sc} and PCE. We use hole-only devices with the structure of ITO/PEDOT:

PSS/active-layer/MoO_3/Al to explore the charge transport in the ternary and binary solar cells. As shown in **Figure S7** and **Table S7**, the hole mobility of the 20% PBDTTS-FTAZ ternary solar cell is slightly increased compared to the binary PTB7-Th:$PC_{71}BM$ from 5.5×10^{-5} cm^2/Vs to 8.9×10^{-5} cm^2/Vs, but then decreases with increased PBDTTS-FTAZ content. The enhanced hole mobility will contribute to an increase of J_{sc} and (together with the enhanced FF) can also help explain the increase in high wavelength EQE of the 20% PBDTTS-FTAZ ternary solar cell with the binary solar cell of PTB7-Th: $PC_{71}BM$.

Recombination dynamics was also investigated by measuring J_{sc} as a function of illumination intensity as shown in **Figure 4d**. J_{sc} follows a power law dependence on light intensity which can be expressed $J_{sc} \propto (P_{light})^{\alpha}$. In general, linear scaling of photocurrent with P_{light} would suggest weak bimolecular recombination and the exponential factor α would be close to 1.0, while sublinear scaling of photocurrent with P_{light} indicates partial loss of charge carries during the charge transport process due to bimolecular recombination. The exponential factors α for all binary solar cells and ternary solar cells with 20% and 80% PBDTTS-FTAZ are 1.03, indicating weak bimolecular recombination both in ternary and relative binary solar cells, as expected given that $E_{ICT+,D} \approx E_{ICT-,A}$.

We have demonstrated that the donor polymer excitons are efficiently quenched forming polymer/fullerene charge transfer excitons that in turn efficiently dissociate into free charges. The generation of charge transfer excitons at the polymer/fullerene interfaces from donor polymer excitons can follow several mechanisms, however. For our ternary system, an exciton on the high band gap polymer (PBDTTS-FTAZ) can Förster transfer (energy transfer) to the low bandgap polymer (PTB7-Th) due to the well-matched PL and absorption spectra. As the two polymers share the same positive pinning energy, the hole of an exciton or a hole-polaron freely can be transferred between the two donors. The difference in band gap also means that electron transfer from PBDTTS-FTAZ to PTB7-Th can occur, giving the

possibility of Dexter-type energy transfer as well, from the high band gap polymer to the low band gap polymer. PL and TRPL were employed to study the possible energy/charge transfer mechanism, shorter PL life time of PTB7-Th: PBDTTS-FTAZ (<2 ps) blend films compared with pure PBDTTS-FTAZ, and completely quenched PL of PBDTTS-FTAZ in the range of 600 to 700 nm in all PTB7-Th: PBDTTS-FTAZ blends (**Figure S6a**) indicates that energy/charge transfer from PBDTTS-FTAZ to PTB7-Th is highly efficient. PL spectra of the two donor polymers and their blends in different ratio was carried out to identify energy/charge transfer between PBDTTS-FTAZ and PTB7-Th. As shown in **Figure 6a**, PL intensity of PTB7-Th in the blend increases with increasing PBDTTS-FTAZ content, suggesting there is energy transfer from PBDTTS-FTAZ to PTB7-Th. While PL intensity of the blend films with different PBDTTS-FTAZ ratios decreases with increasing of PBDTTS-FTAZ as shown in **Figure 6b**, suggesting some PL quenching channels, such as electron transfer and/or hole transfer between PBDTTS-FTAZ to PTB7-Th exist in the blend films. According to analysis above we can conclude that energy transfer and charge transfer co-exist in the blends of PTB7-Th and PBDTTS-FTAZ (**Figure S6 d**). The PL quenching ratio caused by charge transfer in the blends with 20%, 50% and 80% PBDTTS-FTAZ contents are 47%, 64% and 71% respectively. The increased charge transfer ratio with increasing PBDTTS-FTAZ contents may be correlated with hole transfer from PTB7-Th to PBDTTS-FTAZ. The energy transfer and charge transfer between PTB7-Th and PBDTTS-FTAZ make the exciton decay of PBDTTS-FTAZ faster compared to pure PBDTTS-FTAZ as proved by TRPL (**Figure S6b).** Based on above interaction analysis of two donors we can expect the following working process of ternary solar cells (**Figure S6d**): (1) The increased exciton generation of PBDTTS-FTAZ can dissociate at the interface of PBDTTS-FTAZ and $PC_{71}BM$, also confirmed by the redshift in electroluminescence of the charge transfer states and below bandgap EQE spectrum (**Figure S8**) (2) The excited PBDTTS-FTAZ can transfer energy or charges to PTB7-Th and the exciton dissociate at the interface between PTB7-Th and

$PC_{71}BM$. EQE spectra shown in **Figure 4b** confirm that the introduction of PBDTTS-FTAZ improves the EQE between 450nm to 600nm, and the EQE value of ternary solar cell with 20% PIDTTS-FTAZ over the whole wavelength is enhanced.

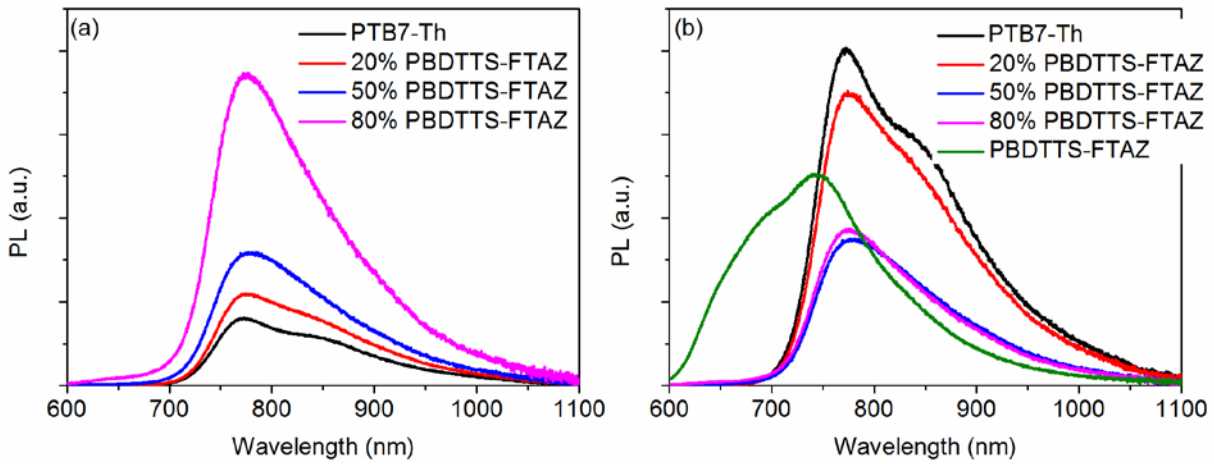

Figure 6. Photoluminescence properties of neat PTB7-Th, PBDTTS-FTAZ films and blend of PTB7-Th: PBDTTS-FTAZ films excited at 450 nm a) Normalized to absorption of PTB7-Th in the blend film. b) Normalized to absorption of the whole film. PL quenching efficiency caused by charge transfer was calculated according to the formula of $(PL_{PTB7\text{-}Th} - PL_{blend})/(PL_{PTB7\text{-}Th}*R)$ where $PL_{PTB7\text{-}Th}$ and PL_{blend} are integrated the PL counts of each pure and blend films. R is the absorption contribution of PBDTTS-FTAZ in the blend at a particular excitation wavelength.

The morphology of the ternary films also is important for device performance, and we explore it using tapping-mode atom force microscopy (AFM), resonant soft X-ray scattering (R-SoXS), grazing incidence wide angle X-ray scattering (GIWAXS), UPS and contact angle measurement. The AFM results indicate a slight increase in the root mean-square (RMS) roughness value and hence domain size in the ternary films compared to the respective binary donor: fullerene films, see **FigureS9** and **TableS8**. The lateral phase separation of the blended thin films was studied using resonant soft X-ray scattering (RSoXS) at 284.2 eV and the scattering profiles are shown in **Figure 7a**. For the corresponding binary blend films PTB7-Th: $PC_{71}BM$ and PBDTTS-FTAZ: $PC_{71}BM$, a strong scattering at 0.18 nm^{-1} and 0.15 nm^{-1} is observed, which translate to a distance of 35 nm and 42 nm respectively. When PBDTTS-

FTAZ and PTB7-Th is blended together, the scattering peak shifts to lower q with increasing of PBDTTS-FTAZ content, suggesting the formation of larger domain sizes than in the binary blend films, consistent with the AFM measurement. Furthermore, multi-scale phase separation appears in the ternary blends as indicated by the larger q value at 284.2 eV compared to other resonant energy and strong scattering curves at 284.2 eV compared to 270 eV (**Figure S10**). Because there is an off-resonate energy of 270eV and the scattering intensity is due to surface roughness contrast. 2D-GIWAXS patterns of binary blend films and the ternary blend films with different content of PBDTTS-FTAZ were performed to investigate the molecular ordering and orientation (**Figure S11**). As shown in corresponding in plane and out of plane scattering profiles in **Figure 7b**, all blend films feature weak diffraction (100) at $q_{xy} \sim 0.3 Å^{-1}$ and (010) at $q_z \sim 1.75 Å^{-1}$, which can be interpret as lamellar stacking with $d_{100} \sim 21 Å$ and π-π stacking with $d_{010} \sim 3.6 Å$. The (010) peak for all blend films in the out-of-plane direction is stronger than in the in-plane direction, implying that both of the binary and ternary blend films exhibit face-on molecular orientation with respect to the substrate and the addition of PBDTTS-FTAZ does not disturb the stacking structure of the host PTB7-Th:$PC_{71}BM$ binary solar cell.

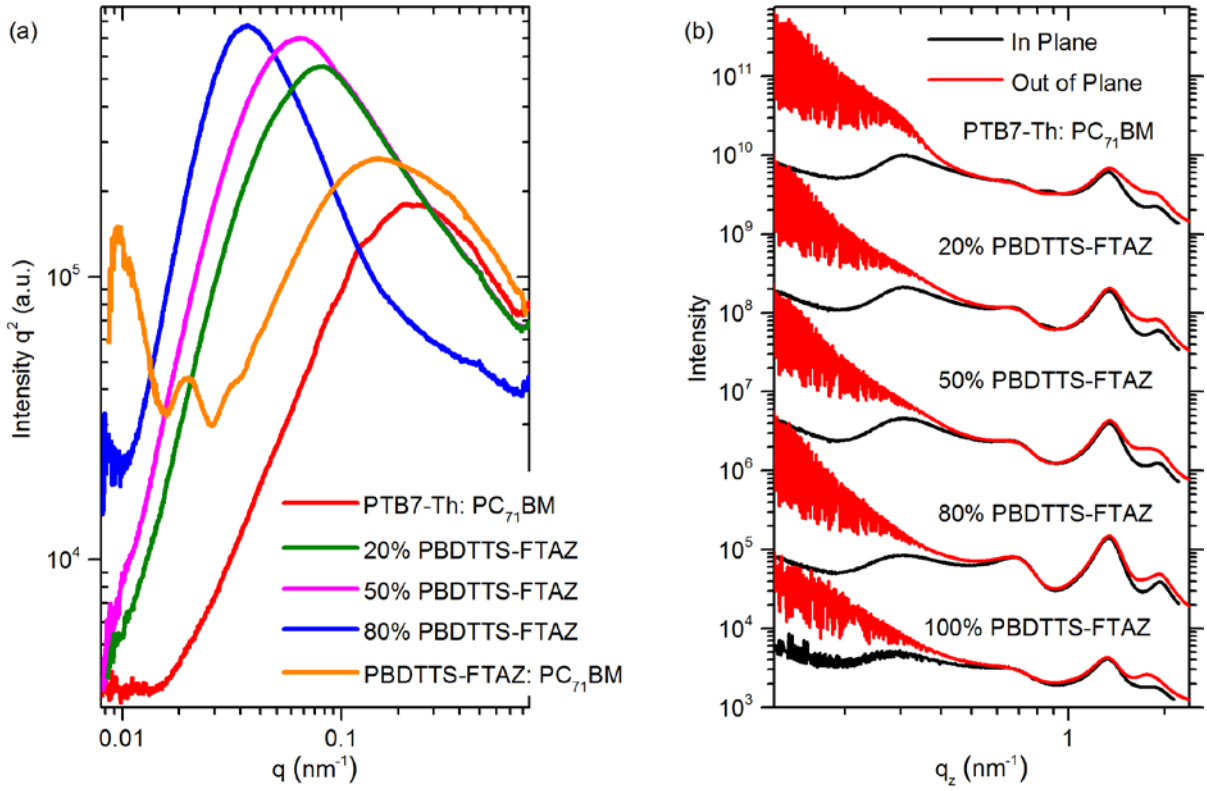

Figure 7. a) R-SoXS profiles for binary and ternary blend films. b) Out of plane and in plane line cuts of ternary and relative binary blend films from 2D GIWAXS.

The surface energy of different component in a blend film is the main driving force for the vertical phase separation,[50] and it also is another driving force that determine the location of the third component in ternary blend.[51, 52] The resulting ternary film component mixing significantly influences exciton dissociation and charge transport and hence the performance of the ternary solar cells. The surface energy of each component is estimated from the water contact angle.[53] The advanced water contact angle of the $PC_{71}BM$, PTB7-Th and PBDTTS-FTAZ is 85.5°, 95.2° and 99.9° as shown in **Table S9**. The corresponding estimated surface energy then is 31.39 mJ/m^2, 25.29 mJ/m^2 and 22.38 mJ/m^2 respectively, We estimate the vertical phase separation in the ternary devices by calculation of the wetting coefficient for PBDTTS-FTAZ in the blend of the PTB7-Th and $PC_{71}BM$ from the interfacial surface energy [54] based on Neumann's equation.[53] The interfacial surface energy is deduced from the surface energy according to Young's equation.[53] The wetting coefficient of the PBDTTS-

FTAZ in the blend of PTB7-Th and $PC_{71}BM$ is around 1.96, which indicates that the PBDTTS-FTAZ tend to be embedded together with PTB7-Th, forming mixed donor polymer domains that based on their surface energies should preferentially segregate at the air/film interfaces.

3. Conclusions

We use a high band gap polymer PBDTTS-FTAZ and a low bandgap polymer PTB7-Th featuring complementary absorption spectra and having identical bulk ionization potential and interface positive pinning energy to fabricate high efficiency fullerene-based ternary solar cells demonstrating a new strategy to design efficient ternary solar cells. We show that selecting donor polymers of identical ionization potential and positive pinning energy delivers efficient hole-transfer between different polymers in mixed domains and between pure polymer domains, thus enabling efficient hole-transport. Matching the donor positive pinning energy to the acceptor negative pinning energy also reduces charge recombination and minimizes V_{oc} loss, and furthermore assists in the dissociation of photogenerated charge transfer excitons into free charges, and all polymer donor and fullerene acceptor excitons can be dissociated more efficiently compared to relative binary solar cells, all of benefit to ternary solar cell performance. We additionally show that energy transfer and charge transfer between the two donor polymers coexist and the ratio of each process is affected by the ratio of two polymers in the blends.

4. Experimental Section

4.1 UPS measurement

Ultraviolet photoelectron spectroscopy (UPS) measurements used for vertical distribution characterization were performed using monochromatized HeI radiation ($h\nu$ = 21.2 eV) in a dedicated home designed and built spectrometer. UPS measurements used for ionization potential (*IP*) and integer charge transfer energy (E_{ICT}) determination were performed using a

Scienta-200 analyzer and HeI radiation. E_{ICT} was deduced from the work function of different substrates covered by thin film derived from the secondary electron cut-off. The ionization potential is determined from the frontier edge of the occupied density states.

4.2 PSC fabrication and characterization.

The structure of the polymer solar cell was Glass/ITO/PEDOT: PSS/polymer: $PC_{71}BM$/LiF/Al. As a buffer layer, PEDOT:PSS (Baytron P VP Al 4083) was spin-coated onto ITO-coated glass substrates, followed by annealing at 120 °C for 15 minutes to remove the water. The thickness of the PEDOT: PSS layer was around 30 nm, as determined by a Dektak 6 M surface profile meter. The active layer, consisting of a copolymer and $PC_{71}BM$ blend, was spin-coated from *o*-dichlorobenzene (*o*DCB) solution onto the PEDOT: PSS layer. The spin-coating was done in a glove box and the prepared active layers were directly transferred to a vapor deposition system mounted inside of the glove box. LiF (0.6 nm) and Al (100 nm) were used as the top electrodes, and deposited via a mask under vacuum onto the active layer. The accurate area of every device (4.6 mm^2), defined by the overlap of the ITO and metal electrode, was measured using a microscope. The PCEs were calculated from the *J–V* characteristics recorded by a Keithley 2400 source meter under the illumination of an AM 1.5G solar simulator with an intensity of 100 mW cm^{-2} (Model SS-50A, Photo Emission Tech., Inc.). The light intensity was determined using a standard silicon photodiode.

4.3 Hole mobility characterization.

The hole mobility of the D/A blend films was measured using the space charge limited current (SCLC) method. The structure of hole-only device is ITO/ PEDOT: PSS /active-layer/MoO_3 /Al. The mobility was determined by fitting the dark current to the model of a single carrier SCLC, which is described by the equation:

$$J = \frac{9}{8}\varepsilon_0\varepsilon_r\mu_h\frac{V^2}{d^3}$$

where J is the current, μ_h is the charge mobility at zero field, ε_0 is the free-space permittivity,

ε_r is the relative permittivity of the material, d is the thickness of the active layer, and V is the effective voltage $V–V_{bi}$, where is the built in voltage. The hole-mobility can be fit from the log $J – V$ curve.

4.4 Optical simulations

Optical constants of two binary blend films PTB7-Th: PC71BM, PBDTTS-FTAZ: $PC_{71}BM$ and ternary blend film with 20% PBDTTS-FTAZ was determined by variable angle spectroscopic ellipsometry using a RC2 ellipsometer from J.A. Woollam Co., Inc. (USA). Measurments were performed at 45, 55, 65 and 75 degrees incident angle on films preperad with identical processing conditions as solar cells on silicon substrates. The optical constants were modelled with the software CompleteEASE from J.A. Woollam Co., Inc (USA) using Kramers-Kronig consistent B-splines. The modelled extinction coefficients were confirmed with the extinction coefficient calculated from the absorption coefficient determined by the Beer-Lambert law from UV/Vis transmission and reflection measurements. The maximum attainable photo current was calculated with a home written transfer matrix method TMM Matlab code calculating the absorption in the active layer as a function of active layer thickness assuming 100% internal photon to electron conversion.

4.5 AFM characterization.

Tapping-mode atomic force microscopy (AFM) images were acquired with an Agilent-5400 scanning probe microscope using a Nanodrive controller with MikroMasch NSC-15 AFM tips and resonant frequencies of ~300 kHz.

4.6 Resonate soft X-ray scattering (R-SoXS) characterization.

R-SoXS transmission measurements were performed at beamline 11.0.1.2[55] at the Advanced Light Source (ALS). Samples for R-SoXS measurements were prepared on a PSS modified Si substrate under the same conditions as those used for device fabrication, and then transferred by floating in water to a 1.5 mm × 1.5 mm, 100 nm thick Si_3N_4 membrane supported by a 5 mm × 5 mm, 200 μm thick Si frame (Norcada Inc.). 2-D scattering patterns were collected on

an in-vacuum CCD camera (Princeton Instrument PI-MTE). The sample detector distance was calibrated from diffraction peaks of a triblock copolymer poly(isoprene-b-styrene-b-2-vinyl pyridine), which has a known spacing of 391 Å. The beam size at the sample is approximately 100 μm by 200 μm.

4.7 Grazing incidence wide-angle X-ray scattering (GIWAXS) characterization.

GIWAXS characterization of the thin film were performed at beamline 7.3.3 at the Advanced Light Source.[56] Samples were prepared on Si substrates using identical blend solutions as those used in devices. The 10 keV X-ray beam was incident at a grazing angle of 0.12°-0.16°, selected to maximize the scattering intensity from the samples. The scattered x-rays were detected using a Dectris Pilatus 2M photon counting detector. The data was processed and analyzed using the NIKA software package.

4.8 Contact angle measurement

Water contact angle was measured on a spin-coated film of corresponding material by CAM 200 optical contact angle meter using pure water. The surface energy and interfacial energy between two different materials were evaluated from contact angle and surface energy. The wetting coefficient of PBDTTS-FTAZ was deduced from interfacial energy.

Supporting Information

Supporting Information is available from the Wiley Online Library or from the author.

Acknowledgements

The work was financed by the Knut and Alice Wallenberg Foundation project “Tail of the Sun”, the Swedish Research Council project grant No. 2016-05498, the Swedish Government Strategic Research Area in Materials Science on Functional Materials at Linköping University (Faculty Grant SFO Mat LiU No 2009 00971) and the Göran Gustafsson Foundation for Research in Natural Sciences and Medicine. This work was supported by Ministry of science and technology (No. 2016YFA0200700), NSFC (21504066, 21534003, 51320105014). X-ray data was acquired at beamlines 7.3.3 and 11.0.1.2 at the Advanced Light Source, which is supported by the Director, Office of Science, Office of Basic Energy Sciences, of the U.S. Department of Energy under Contract No. DE-AC02-05CH11231. The authors thank Chenhui Zhu at beamline 7.3.3, and Cheng Wang at beamline 11.0.1.2 for assistance with data acquisition. CW thanks the China Scholarship Council for a stipend.

Received: ((will be filled in by the editorial staff))
Revised: ((will be filled in by the editorial staff))
Published online: ((will be filled in by the editorial staff))

References

[1] Q. Y. Bao, O. Sandberg, D. Dagnelund, S. Sanden, S. Braun, H. Aarnio, X. J. Liu, W. M. M. Chen, R. Osterbacka, M. Fahlman, *Adv. Funct. Mater.* **2014**, *24*, 6309.
[2] C. Wang, X. Xu, W. Zhang, S. B. Dkhil, X. Meng, X. Liu, O. Margeat, A. Yartsev, W. Ma, J. Ackermann, E. Wang, M. Fahlman, *Nano Energy* **2017**, *37*, 24.
[3] S. Braun, W. R. Salaneck, M. Fahlman, *Adv. Mater.* **2009**, *21*, 1450.
[4] Q. Y. Bao, S. Fabiano, M. Andersson, S. Braun, Z. Y. Sun, X. Crispin, M. Berggren, X. J. Liu, M. Fahlman, *Adv. Funct. Mater.* **2016**, *26*, 1077.
[5] C. Tengstedt, W. Osikowicz, W. R. Salaneck, I. D. Parker, C. H. Hsu, M. Fahlman, *Appl. Phys. Lett.* **2006**, *88*, 053502.
[6] R. J. Davis, M. T. Lloyd, S. R. Ferreira, M. J. Bruzek, S. E. Watkins, L. Lindell, P. Sehati, M. Fahlman, J. E. Anthony, J. W. P. Hsu, *J. Mater. Chem. A* **2011**, *21*, 1721.
[7] M. Fahlman, P. Sehati, W. Osikowicz, S. Braun, M. P. de Jong, G. Brocks, *J. Electron Spectrosc. Relat. Phenom.* **2013**, *190*, 33.
[8] M. T. Greiner, M. G. Helander, W. M. Tang, Z. B. Wang, J. Qiu, Z. H. Lu, *Nat. Mater.* **2012**, *11*, 76.
[9] M. Bokdam, D. Cakir, G. Brocks, *Appl. Phys. Lett.* **2011**, *98*, 113303.
[10] M. Oehzelt, N. Koch, G. Heimel, *Nat. Commun.* **2014**, *5*, 4174.
[11] L. Ley, Y. Smets, C. I. Pakes, J. Ristein, *Adv. Funct. Mater.* **2013**, *23*, 794.
[12] B. Yang, F. W. Guo, Y. B. Yuan, Z. G. Xiao, Y. Z. Lu, Q. F. Dong, J. S. Huang, *Adv. Mater.* **2013**, *25*, 572.
[13] S. K. M. Jonsson, E. Carlegrim, F. Zhang, W. R. Salaneck, M. Fahlman, *Jpn. J. Appl. Phys. part 1* **2005**, *44*, 3695.
[14] K. Vandewal, S. Albrecht, E. T. Hoke, K. R. Graham, J. Widmer, J. D. Douglas, M. Schubert, W. R. Mateker, J. T. Bloking, G. F. Burkhard, A. Sellinger, J. M. J. Frechet, A. Amassian, M. K. Riede, M. D. McGehee, D. Neher, A. Salleo, *Nat. Mater.* **2014**, *13*, 63.
[15] H. Aarnio, P. Sehati, S. Braun, M. Nyman, M. P. de Jong, M. Fahlman, R. Osterbacka, *Adv. Energy Mater.* **2011**, *1*, 792.
[16] V. I. Arkhipov, P. Heremans, H. Bassler, *Appl. Phys. Lett.* **2003**, *82*, 4605.
[17] Q. An, F. Zhang, J. Zhang, W. Tang, Z. Deng, B. Hu, *Energy Environ. Sci.* **2016**, *9*, 281.
[18] Y. Yang, W. Chen, L. Dou, W.-H. Chang, H.-S. Duan, B. Bob, G. Li, Y. Yang, *Nat. Photonics* **2015**, *9*, 190.
[19] L. Lu, T. Xu, W. Chen, E. S. Landry, L. Yu, *Nat. Photonics* **2014**, *8*, 716.
[20] P. K. Tayebeh Ameri, Jie Min , and Christoph J. Brabec, *Adv. Mater.* **2013**, *25*.
[21] N. Felekidis, E. Wang, M. Kemerink, *Energ Environ. Sci.* **2016**, *9*, 257.
[22] Q. S. An, F. J. Zhang, L. L. Li, J. Wang, Q. Q. Sun, J. Zhang, W. H. Tang, Z. B. Deng, *Acs Appl. Mater. Interfaces* **2015**, *7*, 3691.
[23] P. Cheng, Y. Li, X. Zhan, *Energ Environ. Sci.* **2014**, *7*, 2005.
[24] P. Cheng, C. Yan, Y. Wu, J. Wang, M. Qin, Q. An, J. Cao, L. Huo, F. Zhang, L. Ding, Y. Sun, W. Ma, X. Zhan, *Adv. Mater.* **2016**, *28*, 8021.
[25] Y. S. Chen, P. Ye, Z. G. Zhu, X. L. Wang, L. Yang, X. Z. Xu, X. X. Wu, T. Dong, H. Zhang, J. H. Hou, F. Liu, H. Huang, *Adv. Mater.* **2017**, *29*.

[26] Z. S. Peng, Y. X. Xia, F. Gao, K. Xiong, Z. H. Hu, D. I. James, J. W. Chen, E. G. Wang, L. T. Hou, *J. Mater. Chem. A* **2015**, *3*, 18365.
[27] M. An, F. Xie, X. Geng, J. Zhang, J. Jiang, Z. Lei, D. He, Z. Xiao, L. Ding, *Adv. Energy Mater.* **2017**, 1602509.
[28] T. Kumari, S. M. Lee, S.-H. Kang, S. Chen, C. Yang, *Energy Environ. Sci.* **2017**, *10*, 258.
[29] L. Nian, Z. H. Chen, S. Herbst, Q. Y. Li, C. Z. Yu, X. F. Jiang, H. L. Dong, F. H. Li, L. L. Liu, F. Wurthner, J. W. Chen, Z. Q. Xie, Y. G. Ma, *Adv. Mater.* **2016**, *28*, 7521.
[30] T. Liu, X. Pan, X. Meng, Y. Liu, D. Wei, W. Ma, L. Huo, X. Sun, T. H. Lee, M. Huang, H. Choi, J. Y. Kim, W. C. Choy, Y. Sun, *Adv. Mater.* **2017**, *29*, 1604251.
[31] T. Liu, Y. Guo, Y. Yi, L. Huo, X. Xue, X. Sun, H. Fu, W. Xiong, D. Meng, Z. Wang, F. Liu, T. P. Russell, Y. Sun, *Adv. Mater.* **2016**, *28*, 10008.
[32] T. Liu, X. Xue, L. Huo, X. Sun, Q. An, F. Zhang, T. P. Russell, F. Liu, Y. Sun, *Chem. Mater.* **2017**.
[33] T. Kumari, S. M. Lee, S. H. Kang, S. Chen, C. Yang, *Energ Environ. Sci.* **2017**, *10*, 258.
[34] W. Zhao, S. Li, S. Zhang, X. Liu, J. Hou, *Adv. Mater.* **2017**, *29*.
[35] H. Kang, K. H. Kim, T. E. Kang, C. H. Cho, S. Park, S. C. Yoon, B. J. Kim, *Acs Appl. Mater. Interfaces* **2013**, *5*, 4401.
[36] W. Chen, T. Xu, F. He, W. Wang, C. Wang, J. Strzalka, Y. Liu, J. G. Wen, D. J. Miller, J. H. Chen, K. L. Hong, L. P. Yu, S. B. Darling, *Nano Lett.* **2011**, *11*, 3707.
[37] L. Y. Lu, W. Chen, T. Xu, L. P. Yu, *Nat. Commun.* **2015**, *6*, 7327.
[38] L. Ye, S. Q. Zhang, W. C. Zhao, H. F. Yao, J. H. Hou, *Chem. Mater.* **2014**, *26*, 3603.
[39] Z. C. He, B. Xiao, F. Liu, H. B. Wu, Y. L. Yang, S. Xiao, C. Wang, T. P. Russell, Y. Cao, *Nat. Photonics* **2015**, *9*, 174.
[40] Y. Z. Lin, J. Y. Wang, Z. G. Zhang, H. T. Bai, Y. F. Li, D. B. Zhu, X. W. Zhan, *Adv. Mater.* **2015**, *27*, 1170.
[41] T. Liu, L. Huo, X. Sun, B. Fan, Y. Cai, T. Kim, J. Y. Kim, H. Choi, Y. Sun, *Adv. Energy Mater.* **2016**, *6*, 1502109.
[42] Z. Genene, J. Y. Wang, X. Y. Meng, W. Ma, X. F. Xu, R. Q. Yang, W. Mammo, E. G. Wang, *Adv. Electron. Mater.* **2016**, *2*, 160084.
[43] H. J. Bin, Z. G. Zhang, L. Gao, S. S. Chen, L. Zhong, L. W. Xue, C. Yang, Y. F. Li, *J. Am. Chem. Soc.* **2016**, *138*, 4657.
[44] Y. K. Yang, Z. G. Zhang, H. J. Bin, S. S. Chen, L. Gao, L. W. Xue, C. Yang, Y. F. Li, *J. Am. Chem. Soc.* **2016**, *138*, 15011.
[45] Z. L. Guan, J. B. Kim, H. Wang, C. Jaye, D. A. Fischer, Y. L. Loo, A. Kahn, *Org. Electron.* **2010**, *11*, 1779.
[46] S. H. Liao, H. J. Jhuo, Y. S. Cheng, S. A. Chen, *Adv. Mater.* **2013**, *25*, 4766.
[47] C. H. Cui, W. Y. Wong, Y. F. Li, *Energ Environ. Sci.* **2014**, *7*, 2276.
[48] L. A. A. Pettersson, L. S. Roman, O. Inganas, *J. Appl. Phys.* **1999**, *86*, 487.
[49] P. Sehati, S. Braun, L. Lindell, X. J. Liu, L. M. Andersson, M. Fahlman, *IEEE J. Sel. Top. Quantum Electron.* **2010**, *16*, 1718.
[50] J. S. Kim, P. K. H. Ho, C. E. Murphy, R. H. Friend, *Macromolecules* **2004**, *37*, 2861.
[51] S. Honda, H. Ohkita, H. Benten, S. Ito, *Adv. Energy Mater.* **2011**, *1*, 588.
[52] T. W. Cheng, H. Keskkula, D. R. Paul, *Polymer* **1992**, *33*, 1606.
[53] D. Li, A. W. Neumann, *J. Colloid Interface Sci.* **1990**, *137*, 304.
[54] M. Sumita, K. Sakata, S. Asai, K. Miyasaka, H. Nakagawa, *Polym. Bull.* **1991**, *25*, 265.
[55] E. Gann, A. T. Young, B. A. Collins, H. Yan, J. Nasiatka, H. A. Padmore, H. Ade, A. Hexemer, C. Wang, *Rev. Sci. Instru.* **2012**, *83*, 045110.
[56] A. Hexemer, W. Bras, J. Glossinger, E. Schaible, E. Gann, R. Kirian, A. MacDowell, M. Church, B. Rude, H. Padmore, *J. Phys. Conf. Ser.* **2010**, *247*, 012007.

Ternary solar cells with minimum voltage losses around 0.25 eV is designed by combining two donor polymers with same bulk and interface energy which make the hole transportation like in one donor polymer. The voltage losses was minimized due to $E_{ICT+} \approx E_{ICT-}$, where the trade-off between enhancing of charge generation and charge recombination by ICT states arrives sweet spot.

Keyword: Ternary Solar Cell, Same Bulk and Interface Energy, Binary Equivalent, Minimum Voltage Losses

Chuanfei Wang, Wei Zhang, Xiangyi Meng, Jonas Bergqvist, Xianjie Liu, Zewdneh Genene, Xiaofeng Xu, *Arkady Yartsev, Olle Inganäs, Wei Ma, Ergang Wang, Mats Fahlman**

Ternary Organic Solar Cells with Minimum Voltage Losses

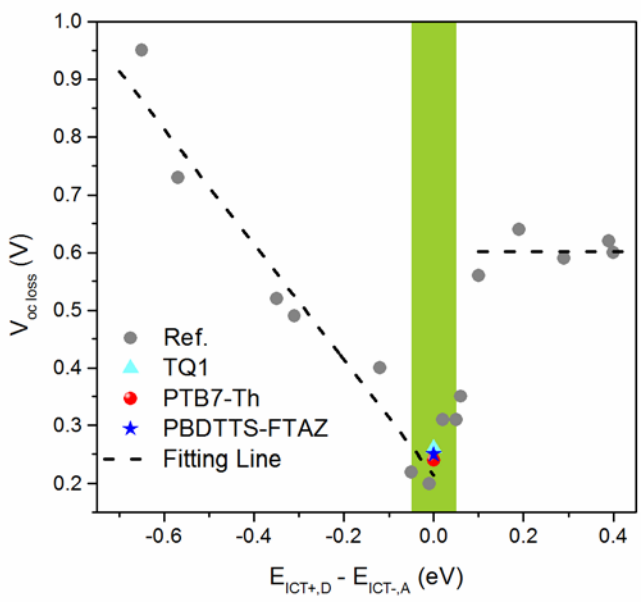

Supporting Information

Ternary Organic Solar Cells with Minimum Voltage Losses

Chuanfei Wang, Wei Zhang, Xiangyi Meng, Jonas Bergqvist, Xianjie Liu, Zewdneh Genene, Xiaofeng Xu, *Arkady Yartsev, Olle Inganäs, Wei Ma, Ergang Wang, Mats Fahlman**

Table of Contents

1. Energy Level Alignment

The ionization energy of molecular orbitals strongly depends on the local environment, *i.e.* the intermolecular order and the nature of surrounding molecules/materials. Hence, though the ionization energies of the various occupied molecular orbitals are well defined for an isolated molecule, in an amorphous or polycrystalline molecular film, there is a broad distribution of ionization energies for each orbital. [1] Even though each molecule has *e.g.* a discrete energy corresponding to the removal of one electron from the highest occupied molecular orbital (HOMO), typically referred to as the Ionization Potential (*IP*) of the molecule, if then each molecule in the film has a unique local environment each *IP* will be unique and there will hence be a distribution of *IP* due to variations in the local molecular order. The same holds true for the unoccupied molecular orbitals, resulting in a distribution of Electron Affinities (*EA*) in the film. The energy gap is then defined by the upper edge of the *IP* energy distribution and the lower edge of the *EA* energy distribution, and there are consequently per definition no gap states in absence of doping or molecular defects as the frontier *IP*/*EA* energies created by variations in molecular order define the actual gap. Organic semiconductors (OSC) films used in organic photovoltaic technologies generally are amorphous or polycrystalline and defects/variation in the local order of OSC film create a distribution of ionization energies. Every polymer in a film thus has its own individual ionization potential (*IP*) and electron affinity (*EA*), with the film *IP* and *EA* then represented by the smallest/largest individual *IP*/*EA*. The frontier parts of the resulting occupied and unoccupied state distributions forming the energy gap are often modeled as being Gaussian. Due to processing conditions relevant to printed electronics, the organic semiconductor films typically are physisorbed on substrates, forming weakly-interacting interfaces. The ICT model was developed to describe energy level alignment at such interfaces and over heterolayer stacks featuring OSC. [2, 3, 4] The ICT model predicts and explains the experimentally verified

abrupt transitions between a vacuum level alignment regime and Fermi-level pinning regimes upon variations of the work function of the substrate. The Fermi-level pinning regimes feature a potential step that scales with the difference between the equilibrium ionization potential or electron affinity of the organic semiconductor at the interface and the work function (Φ_{SUB}) of the substrate. The origin of the potential step (Δ) is explained by spontaneous charge transfer across the interface via tunneling (integer charge transfer) when the substrate work function is higher than the energy required to take away one electron (lower than the energy gained from adding one electron) from (to) the molecule at an interface producing a fully relaxed state. The most easily oxidized donor molecules (or segments on polymers) hence will be "used up" until enough charge has been transferred across the interface to create a potential step that equilibrates the Fermi level. The energy where the Fermi level is subsequently pinned is referred to as $E_{ICT+,-}$ depending on if it is positive or negative polarons that are being created. Unless a crystalline film, the interface polarons will be localized on one or more molecules (depending on local order, orbital overlap etc.), but will not be delocalized over the film in a band-like picture, as there are no bands. Note that the interface charge transfer states do not have the same energy as bulk polarons, mainly due to Coulombic interaction with the opposite charge across the interface and variations in molecular order. Three distinct energy level alignment regimes are predicted by the model at Fermi level equilibrium and are described by: (i) $\Phi_{SUB} < E_{ICT-}$ - Fermi level pinning to a negative integer charge transfer state, resulting in a substrate-independent work function, slope = 0; (ii) $E_{ICT-} < \Phi_{SUB} < E_{ICT+}$ - Vacuum level alignment, giving a substrate-dependent work function, slope = 1; (iii) $\Phi_{SUB} > E_{ICT+}$ - Fermi level pinning to a positive integer charge transfer state, resulting again in a substrate-independent work function slope = 0, see **Figure S1**.

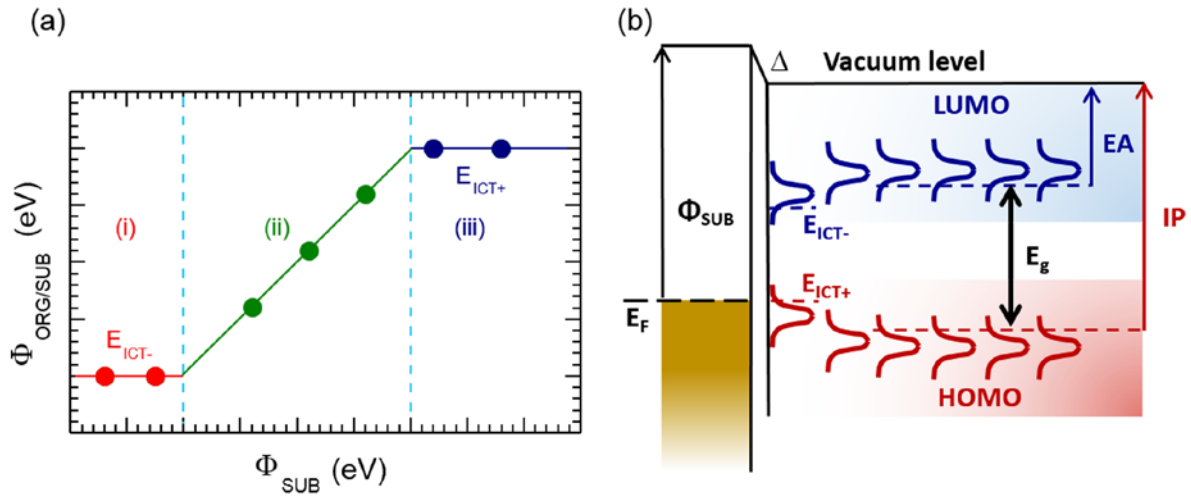

Figure S1. Left panel (a): Typical energy level alignment behavior for weakly interacting organic semiconductor interfaces that follow the ICT model, where the resulting work function ($\Phi_{ORG/SUB}$) is either independent (i, iii) or linearly dependent with a slope of ~1 (ii) of the substrate work function (Φ_{SUB}). Right panel b): Diagram showing energy level alignment including the ICT state and bulk frontier density of state distribution. Here the Fermi level becomes pinned to the E_{ICT+} (oxidation of molecules at the interface causing Fermi level equilibrium).

As mentioned above, the E_{ICT+} (E_{ICT-}) energy is related to the energy required to take away one electron (the energy gained from adding one electron) from (to) the OSC molecule *at an interface* producing a fully relaxed state. These energies are thus similar in nature to but differ from the ionization potential (*IP*) and electron affinity (*EA*) of the organic semiconductor, *i.e.* the polaronic transport states, such as $E_{ICT+} = IP - B^+$ and $E_{ICT-} = EA + B^-$, where B^+ (B^-) is the Coulomb energy associated with charging a molecule in the interface layer with an hole (electron),[4, 5], and are thus moved into the gap compared to the bulk polarons (*IP*/*EA*). Note that *IP*, *EA* and B^+ and B^- are all dependent on the local environment of the molecule, due to screening of the added charge, hence the $E_{ICT+,-}$ also depend on the local environment at the interface (inter- and intramolecular order, etc.). Despite the dependence on local order, fullerenes and conjugated polymers typically display $E_{ICT+,-}$ values independent on the

substrate they are combined with. This may at first glance appear counterintuitive, but is a direct consequence of the non-single-crystalline nature of such films. Unless the surface energy of a particular substrate is radically different, the same types of local molecule order at the interface will be present upon film formation (to greater or lesser degree) and so are then the "most easily oxidized / reduced" sites that participate in the equilibration of the Fermi level. Hence, the $E_{ICT+,-}$ values obtained typically deviate very little (± 0.05 eV) as can be seen from literature even though both organic and inorganic substrates featuring different surface roughness, surface energy and potential for solvent-induced interface intermixing are used.

For a donor/acceptor heterojunction, the donor E_{ICT+} and acceptor E_{ICT-} can be used to determine if there is a charge transfer induced potential step, which not only affects the energy level alignment but also trap-assisted recombination losses in the film. When $E_{ICT-,\,A} \approx E_{ICT+,D}$, trap assistant recombination via occupied ICT states is reduced and the (weak) dipole layer between donor and acceptor induced by ICT assists photogenerated charge transfer exciton dissociating into free charges leading to dramatic increase of fraction G/β in **Equation (S1)**.[6, 7]

$$eVoc = \Delta E_{g,eff}^{DA} - kTln\left(\frac{\beta N_C N_V}{G}\right) = \Delta E_g^{DA} + \Delta - kTln\left(\frac{\beta N_C N_V}{G}\right), \quad \text{Equation (S1)}$$

2. Optical Properties of Two Donor Polymer Blends

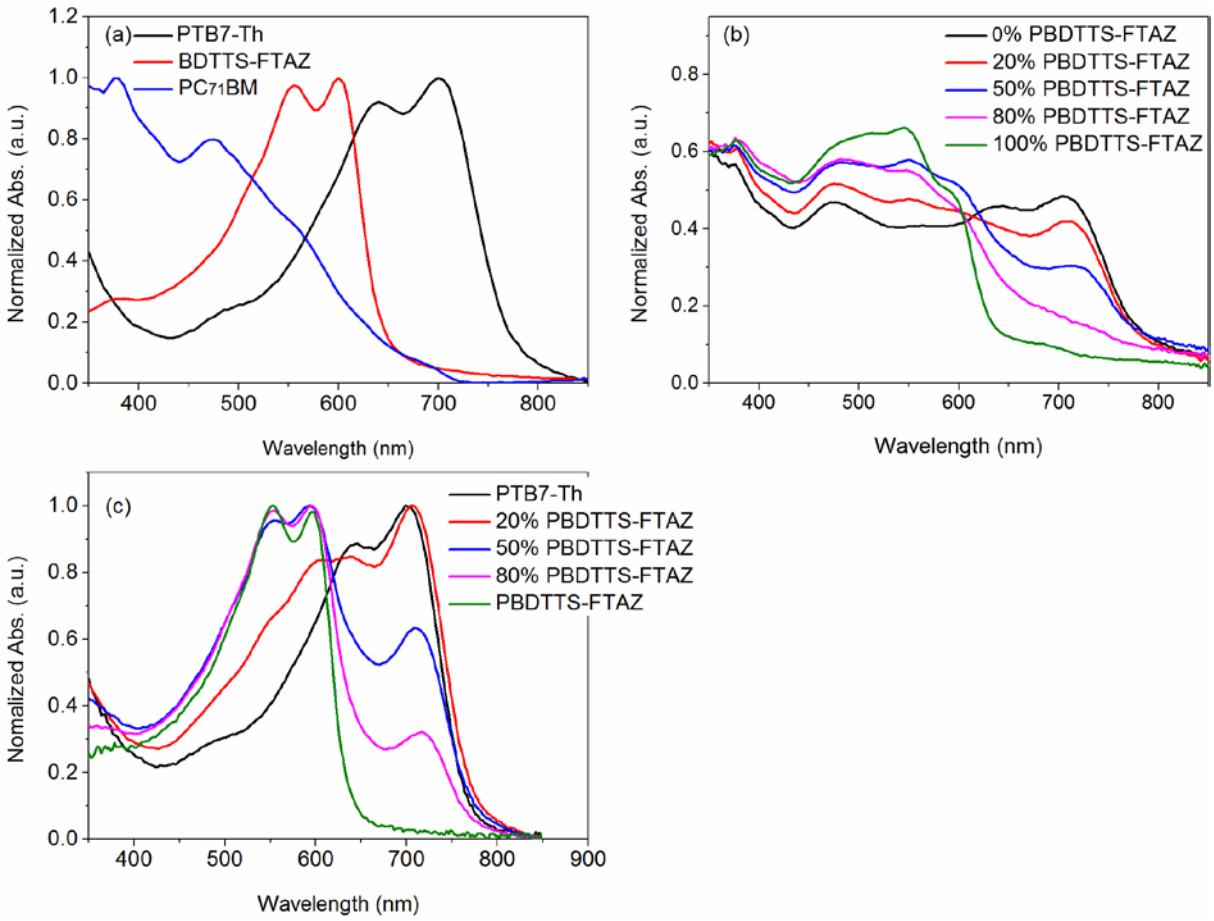

Figure S2. a) Normalized absorption spectrum of pure PTB7-Th, PBDTTS-FTAZ and $PC_{71}BM$ films. b) Normalized absorption spectra of ternary blends with different PBDTTS-FTAZ contents. The D-A ratio is 1:1.5 for all ternary blends. (c) Normalized absorption spectrum of two donor blends.

3. Ultraviolet Photoelectron Spectroscopy (UPS) Measurement and Energy Levels

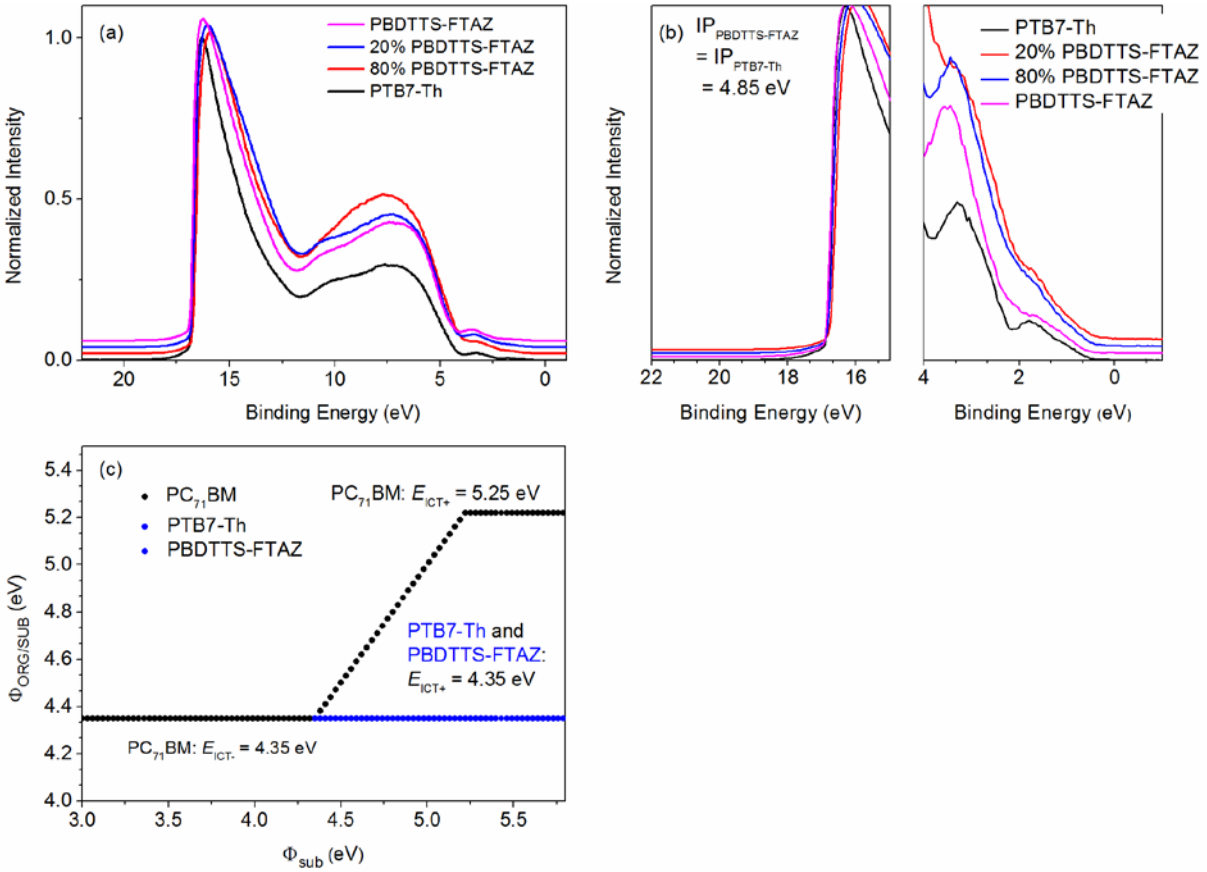

Figure S3. (a), (b) UPS spectra of pure PTB7-Th, Pure PBDTTS-FTAZ, and blend film of PTB7-Th: PBDTTS-FTAZ. c) Dependences of the work function of substrates with overlayer ($\Phi_{org/sub}$) on the work function of the bare substrate (Φ_{sub}).

Bulk energy levels (*IP*) and pinning energies are listed in **Table S1**. The pinning energy of PTB7-Th and PBDTTS-FTAZ are deduced from **FigureS3 (b)**. The work function (WF) of the ITO/PEDOT: PSS is around 4.9 eV, and the work function of the ITO/PEDOT: PSS with overlayers of PTB7-Th or PBDTTS-FTAZ is 4.35 eV (21.2 – 16.85) eV, which gives a positive pinning energy of 4.35 eV. *IP* and E_{ICT-} of $PC_{71}BM$ are in agreement with literature tested in our own lab.[7] The electron affinity (*EA*) were deduced from the ionization potential (*IP*) and absorption onset, *i.e.* $EA = IP + 1240/\lambda_{onset}$.

Table S1. Ionization potential (*IP*) and Pinning Energy (E_{ICT}) deduced from UPS. $\Delta E_g^{DA} = IP_D - EA_A$, $\Delta E_{g,eff}^{DA} = IP_D - EA_A + \Delta$. $\Delta = E_{ICT+} - E_{ICT-}$.

component	E_{ICT+}	E_{ICT-}	*IP*	*EA*	Δ	ΔE_g^{DA}	$\Delta E_{g,eff}^{DA}$
Pure PTB7-Th	4.35	-	4.85	3.27	0	1.05	1.05
Pure PBDTTS-FTAZ	4.35	-	4.85	2.95	0	1.05	1.05
$PC_{71}BM$	5.22	4.35	5.9	3.80[7, 8]	-	-	-
PTB7-Th: PBDTTS-FTAZ = 8:2	4.39	-	4.86	-	-	-	-
PTB7-Th: PBDTTS-FTAZ = 2:8	4.35	-	4.84	-	-	-	-

4. Variation of Photovoltaic Performance of Ternary Solar Cells with Different Contents of PBDTTS-FTAZ.

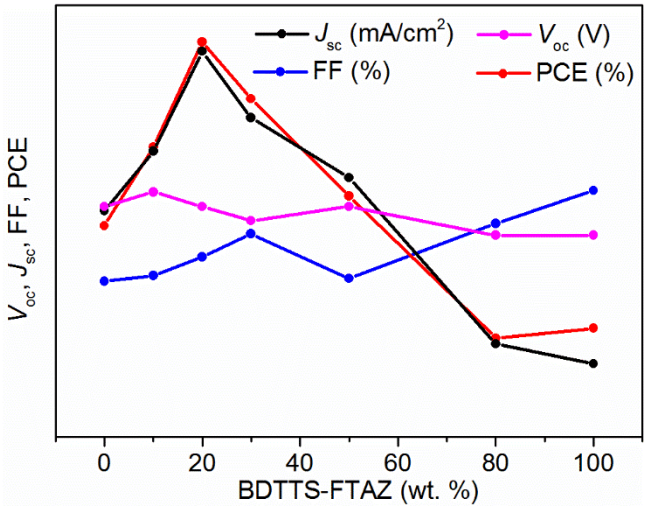

Figure S4. Variation trend of V_{oc}, J_{sc}, FF and PCE with the content of PBDTTS-FTAZ

5. The Theoretical and Experimental J_{sc} as Function of Active Layer Thickness

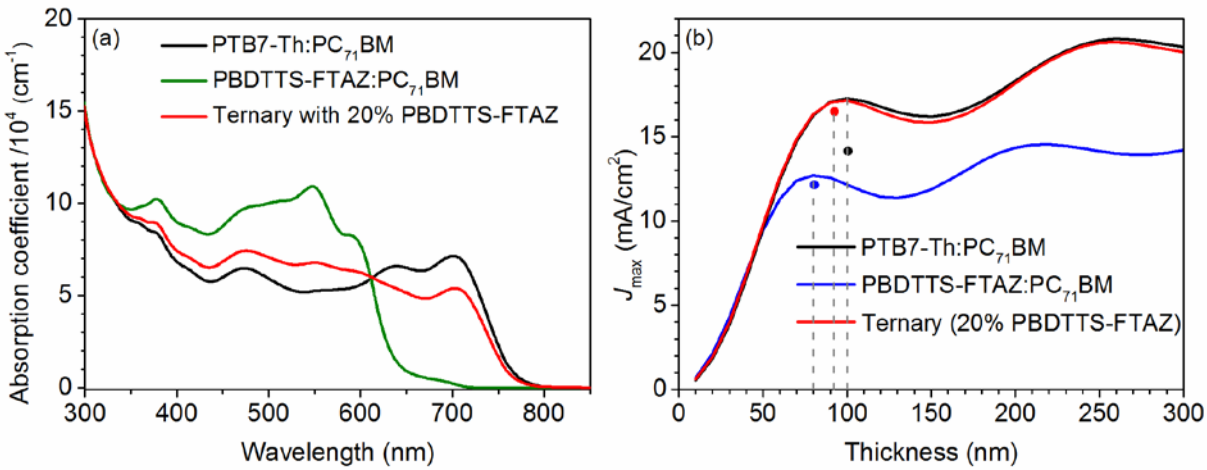

Figure S5. (a) Absorption coefficient of ternary blends with 20% PBDTTS-FTAZ and relative binary blends tested by ellipsometry. (b) $J_{sc\text{-}max}$ predicted by transfer matrix model as a function of the active layer, assuming 100% internal quantum efficiency.

6. Electric Field Dependent Current Density

Table S4. Saturation current density and short circuit current density increments of ternary solar cells with different content of PBDTTS-FTAZ in the blend.

PBDTTS-FTAZ (%)	J_{sc} (mA/cm^2)	J_{sat} (mA/cm^2)	P(E,T)
0	14.40	15.2	94.6%
20	16.75	17.7	94.6%
50	14.91	15.7	94.9%
80	12.42	13.0	95.4%
100	12.05	12.7	94.9%

7. Photoluminescence (PL) Measurement of PTB7-Th and PBDTTS-FTAZ

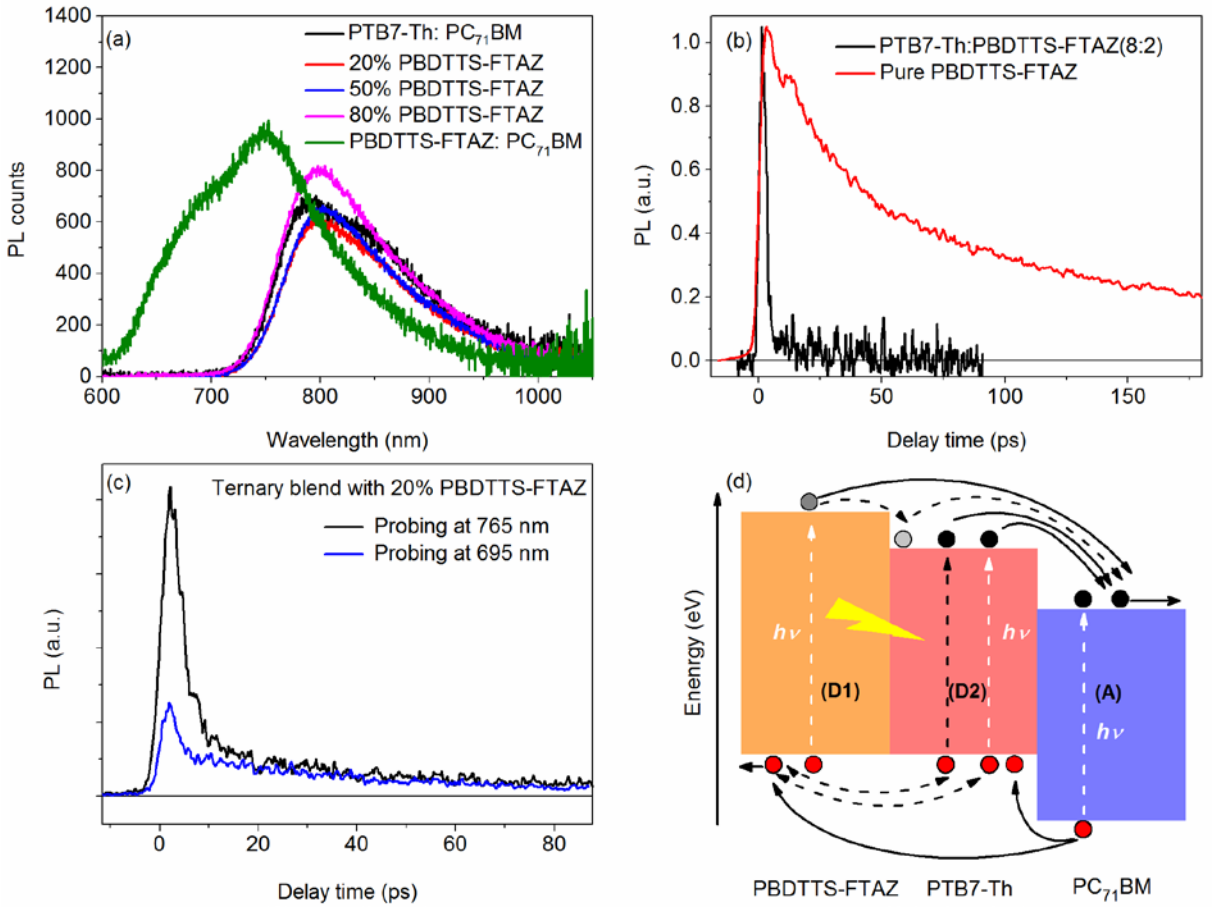

Figure S6. a) The photoluminescence properties of neat PTB7-Th, PBDTTS-FTAZ and blend films of these two donors with different ratio excited at 405 nm. Note that the spectrum was not corrected by absorption here b) TRPL kinetics of PBDTTS in neat, binary blend and c) ternary blend with 20%PBDTTS-FTAZ at different probe wavelengths. d) Diagram of energy and charge transfer involved in ternary blends.

We find that in the ternary blend the amplitude of the faster PL decay component at 765 nm is higher than that at 695nm. At these two wavelengths the emission of $PC_{71}BM$ and PBDTTS-FTAZ are rather similar whereas PTB7-Th emits much stronger close to its PL maximum at 765 nm than at the far blue edge at 695 nm. Thus, at 695 nm we assign the faster PL decay component to PBDTTS-FTAZ and the slower decay to $PC_{71}BM$. At 765 nm, we observe a very similar slow decay component due to $PC_{71}BM$. The fast decay component at 765 nm is therefore attributed to PL signal from both PBDTTS-FTAZ and PTB7-Th. Further, the relative PL amplitudes agree with the blending ratio of the two polymers.

Table S6. Parameters of TRPL measurment

Film	A_1	τ_1 (ps)	A_2	τ_2
PTB7-Th:$PC_{71}BM$ (1:1.5)	1	3.3	0.5	62
PBDTTS-FTAZ:$PC_{71}BM$ (1:1.5)	1.3	3.8	0.3	61
(PTB7-Th:PBDTTS-FTAZ= 8:2):$PC_{71}BM$	3	1.4	0.2	33.8

Fitting equation: $y = A_1\ exp(-t/\tau_1)+A_2\ exp(-t/\tau_2)$, where A is amplitude, and τ is exciton lifetime.

8. Hole Mobility Measurement by Space Charge Limited Current (SCLC) Method

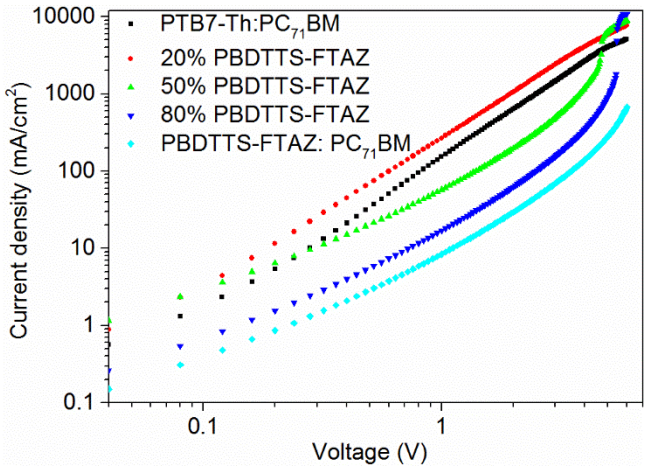

Figure S7. *J–V* characteristic of the referenced binary and ternary blends in hole-only devices measured at room temperature

Table S7. Hole mobility

PBDTTS-FTAZ	μ_{hole} (cm^2/vs)
0%	5.5 × 10-5
20%	8.9 × 10-5
50%	1.1× 10-5
80%	5.3 × 10-6
100%	1.8 × 10-6

9. Electroluminescence (EL) and FTPS-EQE Measurements

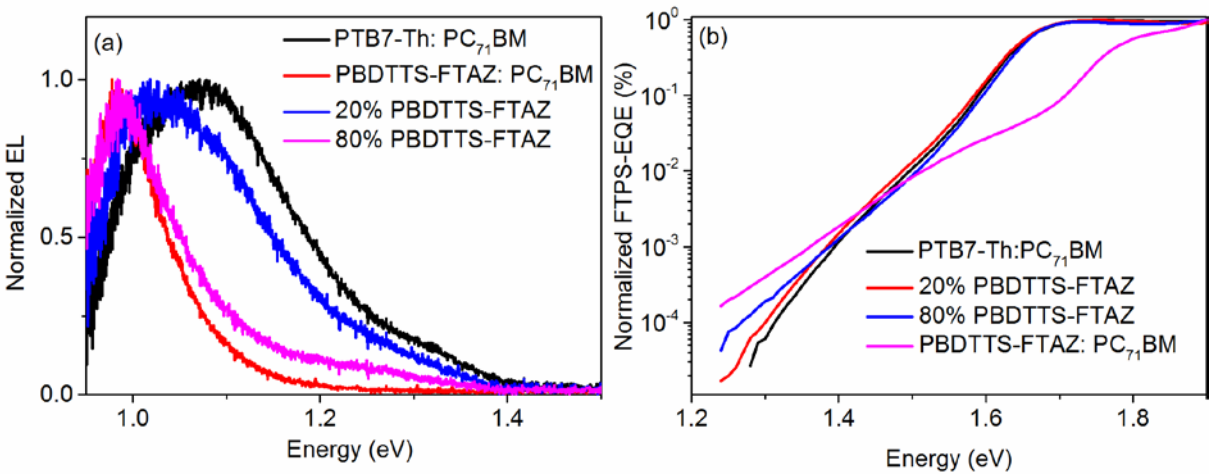

Figure S8. (a) Electroluminescence spectrum under a forward bias and (b) FTPS-EQE spectra of the binary solar cells of PTB7-Th: $PC_{71}BM$, PBDTTS-FTAZ: $PC_{71}BM$ and ternary solar cell with 20% and 80% PBDTTS-FTAZ.

The energy of charge transfer state (E_{CT}) [9, 10, 11] in ternary solar cells are usually in between the E_{CT} of the two corresponding binary solar cells and is typically obtained from electroluminescence (EL) measurements or Fourier-transform photocurrent spectroscopy–external quantum efficiency (FTPS-EQE), see **Figure S8a** and **b** respectively.[10] With increasing PBDTTS-FTAZ content, both of the FTPS-EQE and EL spectra are redshifted but stay in between the spectra of the two binary solar cells, indicating co-existence interaction between two donors and $PC_{71}BM$. [12]

10. Film Morphology Analysis

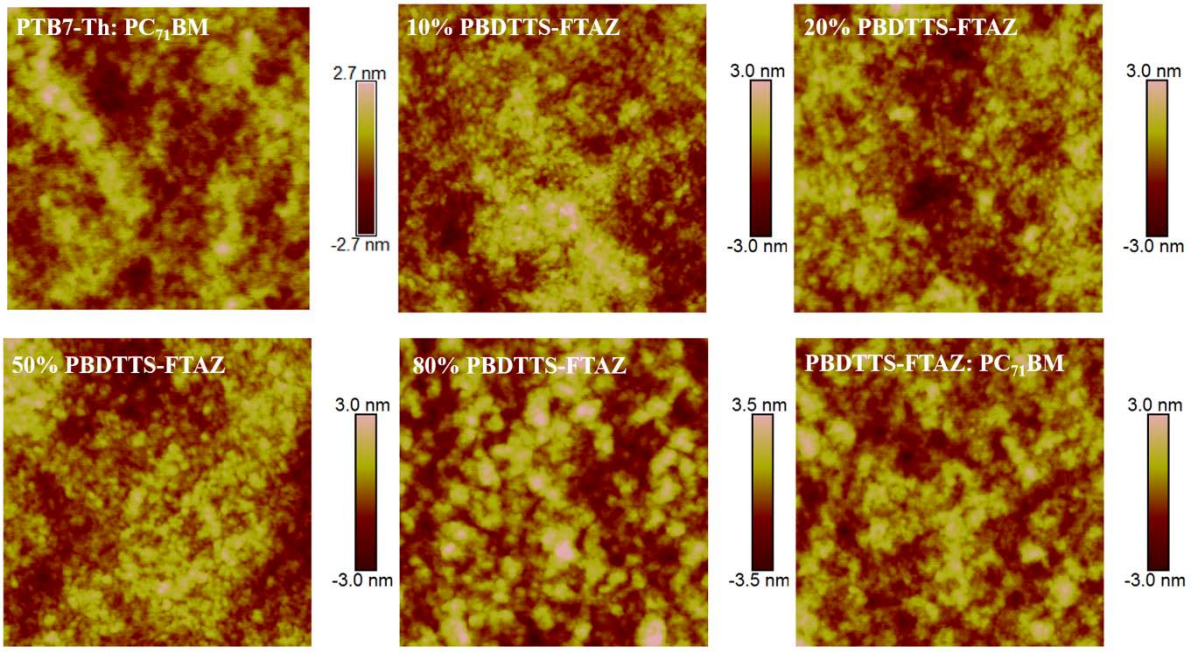

Figure S9. AFM height images (1×1 μm^2) of ternary solar cells with different PBDTTS-FTAZ contents.

Table S8. The root-mean-square (RMS) roughness of the PTB7-Th: PBDTTS-FTAZ: $PC_{71}BM$ blends with different content of PBDTTS-FTAZ.

PBDTTS-FTAZ	Rq (nm)
0%	0.76
10%	0.88
20%	0.88
50%	0.89
80%	1.20
100%	0.85

11. R-SoXS and GIWAXS Characterization

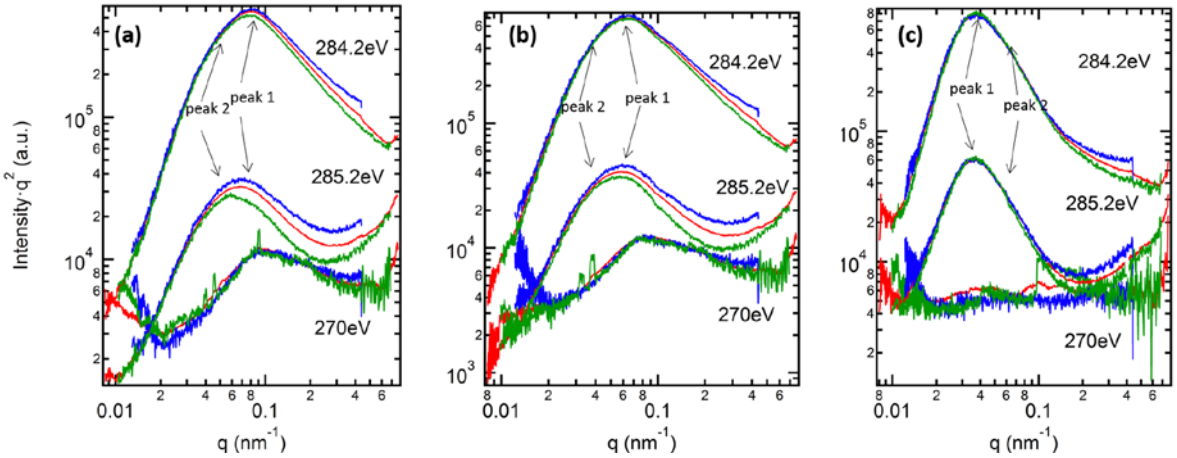

Figure S10. R-SoXS profiles under different resonant energy for (a) 20% PBDTTS-FTAZ (b) 50% PBDTTS-FTAZ and (c) 80% PIDTTS-FTAZ in ternary blends.

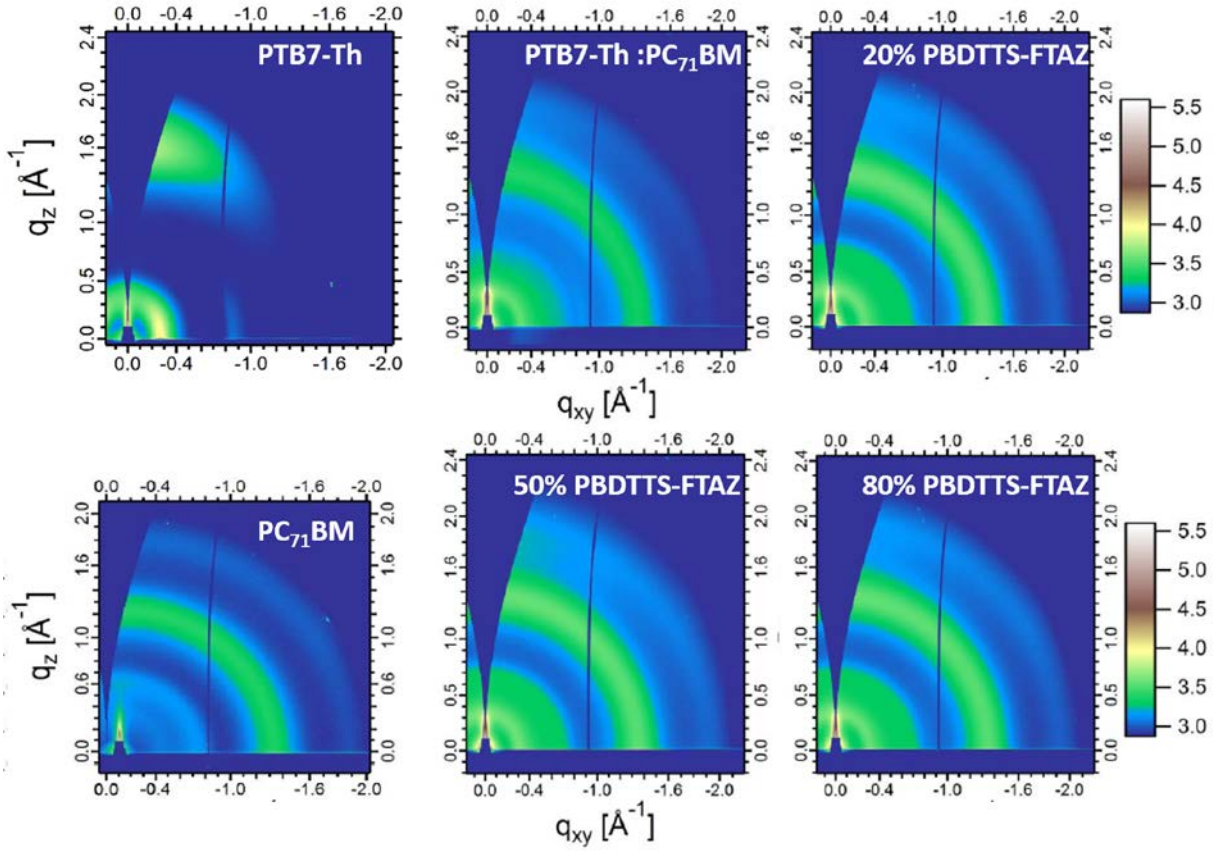

Figure S11. GIWAXS 2D patterns of ternary and referenced binary blend films

12. Contact Angle Measurement and Surface Energy Calculation

Table S9. Water contact angle and corresponding surface energy of neat PTB7-Th, PBDTTS-FTAZ and $PC_{71}BM$ films

Adv.

Contact Angel θ °	Surface tension γ_{sv} **(*mJ/m*^{2})**	Solid liqued tention γ_{sl} **(*mJ/m*^{2})**
85.5	31.39	25.69
95.2	25.29	31.89
99.9	22.38	34.9

The calculation process of wetting coefficient are shown as following

The wetting coefficient of PBDTTS-FTAZ in blends of materials PTB7-Th and $PC_{71}BM$ can be calculated according to **Equation S2** (Young's equation according),[13] where $\omega_{s(c)}$ represent wetting coefficient and $\gamma_{s(X)s(Y)}$ represent interface surface energy between solid X and solid Y, which can be deduced from **Equation S3** (Neumann's equation).[14] γ_{sv} represent surface tension energy between solid(s) and vapor (v), which can be deduced from equation S3 and γ_{lv} represent liquid-vapor surface tension. θ represents the water contact angle of the film. β is 0.000115 m^4mj^{-2} in **Equation S3** and **S7**. The physical meaning and detail derivation process of each equation can be found in literature. When $\omega_{s(C)} < -1$, C (PBDTTS-FTAZ) will be tend to embedded in the domain of material B ($PC_{71}BM$). When $\omega_{s(C)} > 1$, material C (PBDTTS-FTAZ) will be tend to embedded in the domain of material A (PTB7-Th). When $-1 < \omega_{s(C)} < 1$, C (PBDTTS-FTAZ) will be tend to distribute at the interface of material A (PTB7-Th) and material B ($PC_{71}BM$). The wetting coefficient of PBDTTS-FTAZ deduced from advancing water contact angle is 1.96, which means that the PBDTTS-FTAZ would like to embed together with PTB7-Th.

$\omega_{s(C)} = \frac{\gamma_{s(C)s(B)} - \gamma_{s(C)s(A)}}{\gamma_{s(A)s(B)}}$, Equation (S2)

$\gamma_{s(X)s(Y)} = \gamma_{s(X)v} - \gamma_{s(Y)v} - \sqrt{\left(\gamma_{s(X)v}\gamma_{s(Y)v}\right)} * exp\left(-\beta\left(\gamma_{s(X)v}\gamma_{s(Y)v}\right)^2\right)$, Equation (S3)

$\gamma_{sv} = \gamma_{lv}x_{n+1}^2$, Equation (S4)

$x_{n+1} = x_n - \frac{x_n - ae^{b\left(1-x_n^2\right)^2}}{1+4abx_n\left(1-\left(x_n^2\right)e^{b\left(1-x_n^2\right)^2}\right)}$ $(0 \le x \le 1)$, Equation (S5)

$\alpha = \frac{\cos\theta+1}{2}$, Equation (S6)

$b = \beta\gamma_{lv}^2$, Equation (S7)

13. Reference

[1] W. R. Salaneck, *Phys Rev Lett* **1978**, *40*, 60.
[2] S. Braun, W. R. Salaneck, M. Fahlman, *Adv. Mater.* **2009**, *21*, 1450.
[3] M. Fahlman, A. Crispin, X. Crispin, S. K. M. Henze, M. P. de Jong, W. Osikowicz, C. Tengstedt, W. R. Salaneck, *J Phys-Condens Mat* **2007**, *19*.
[4] M. Fahlman, P. Sehati, W. Osikowicz, S. Braun, M. P. de Jong, G. Brocks, *J. Electron Spectrosc. Relat. Phenom.* **2013**, *190*, 33.
[5] M. Bokdam, D. Cakir, G. Brocks, *Appl. Phys. Lett.* **2011**, *98*, 113303.
[6] W. Tress, K. Leo, M. Riede, *Appl. Phys. Lett.* **2013**, *102*.
[7] Q. Y. Bao, O. Sandberg, D. Dagnelund, S. Sanden, S. Braun, H. Aarnio, X. J. Liu, W. M. M. Chen, R. Osterbacka, M. Fahlman, *Adv. Funct. Mater.* **2014**, *24*, 6309.
[8] Z. L. Guan, J. B. Kim, H. Wang, C. Jaye, D. A. Fischer, Y. L. Loo, A. Kahn, *Org. Electron.* **2010**, *11*, 1779.
[9] K. Vandewal, S. Himmelberger, A. Salleo, *Macromolecules* **2013**, *46*, 6379.
[10] K. Vandewal, K. Tvingstedt, A. Gadisa, O. Inganas, J. V. Manca, *Phys. Rev. B* **2010**, *81*.
[11] K. Vandewal, K. Tvingstedt, A. Gadisa, O. Inganas, J. V. Manca, *Nat. Mater.* **2009**, *8*, 904.
[12] S. A. Mollinger, K. Vandewal, A. Salleo, *Adv. Energy Mater.* **2015**, *5*, 1501335.
[13] M. Sumita, K. Sakata, S. Asai, K. Miyasaka, H. Nakagawa, *Polym. Bull.* **1991**, *25*, 265.
[14] D. Li, A. W. Neumann, *J. Colloid Interface Sci.* **1990**, *137*, 304.